Equivariant Flow Matching for Point Cloud Assembly

Anonymous Author(s)
Affiliation
Address
email

Abstract

The goal of point cloud assembly is to reconstruct a complete 3D shape by aligning multiple point cloud pieces. This work presents a novel equivariant solver for assembly tasks based on flow matching models. We first theoretically show that the key to learning equivariant distributions via flow matching is to learn related vector fields. Based on this result, we propose an assembly model, called equivariant diffusion assembly (Eda), which learns related vector fields conditioned on the input pieces. We further construct an equivariant path for Eda, which guarantees high data efficiency of the training process. Our numerical results show that Eda is highly competitive on practical datasets, and it can even handle the challenging situation where the input pieces are non-overlapped.

1 Introduction

Point cloud (PC) assembly is a classic machine learning task which seeks to reconstruct 3D shapes by aligning multiple point cloud pieces. This task has been intensively studied for decades and has various applications such as scene reconstruction [48], robotic manipulation [32], cultural relics reassembly [39] and protein designing [41]. A key challenge in this task is to correctly align PC pieces with small or no overlap region, *i.e.*, when the correspondences between pieces are lacking.

To address this challenge, some recent methods [32, 40] utilized equivariance priors for pair-wise assembly tasks, *i.e.*, the assembly of two pieces. In contrast to most of the state-of-the-art methods [30, 51] which align PC pieces based on the inferred correspondence, these equivariant methods are correspondence-free, and they are guided by the equivariance law underlying the assembly task. As a result, these methods are able to assemble PCs without correspondence, and they enjoy high data efficiency and promising accuracy. However, the extension of these works to multi-piece assembly tasks remains largely unexplored.

In this work, we develop an equivariant method for multi-piece assembly based on flow matching [25]. Our main theoretical finding is that to learn an equivariant distribution via flow matching, one only needs to ensure that the initial noise is invariant and the vector field is related (Thm. 4.2). In other words, instead of directly handling the $SE(3)^N$-equivariance for N-piece assembly tasks, which can be computationally expensive, we only need to handle the related vector fields on $SE(3)^N$, which is efficient and easy to construct. Based on this result, we present a novel assembly model called equivariant diffusion assembly (Eda), which uses invariant noise and predicts related vector fields by construction. Eda is correspondence-free and is guaranteed to be equivariant by our theory. Furthermore, we construct a short and equivariant path for the training of Eda, which guarantees high data efficiency of the training process. When Eda is trained, an assembly solution can be sampled by numerical integration, *e.g.*, the Runge-Kutta method, starting from a random noise.

The contributions of this work are summarized as follows:

Submitted to 39th Conference on Neural Information Processing Systems (NeurIPS 2025). Do not distribute.

- We present an equivariant flow matching framework for multi-piece assembly tasks. Our theory reduces the task of constructing equivariant conditional distributions to the task of constructing related vector fields, thus it provides a feasible way to define equivariant flow matching models.
- Based on the theoretical result, we present a simple and efficient multi-piece PC assembly model, called equivariant diffusion assembly (Eda), which is correspondence-free and is guaranteed to be equivariant. We further construct an equivariant path for the training of Eda, which guarantees high data efficiency.
- We numerically show that Eda produces highly accurate results on the challenging 3DMatch and BB datasets, and it can even handle non-overlapped pieces.

2 Related work

Our proposed method is based on flow matching [25], which is one of the state-of-the-art diffusion models for image generation tasks [11]. Some applications on manifolds have also been investigated [4, 46]. Our model has two distinguishing features compared to the existing methods: it learns conditional distributions instead of marginal distributions, and it explicitly incorporates equivariance priors.

The PC assembly task studied in this work is related to various tasks in literature, such as PC registration [30, 47], robotic manipulation [32, 31] and fragment reassembly [43]. All these tasks aim to align the input PC pieces, but they are different in settings such as the number of pieces, deterministic or probabilistic, and whether the PCs are overlapped. More details can be found in Appx. A. In this work, we consider the most general setting: we aim to align multiple pieces of non-overlapped PCs in a probabilistic way.

Recently, diffusion-based methods have been proposed for assembly tasks, such as registration [6, 18, 44] manipulation [32] and reassembly [34, 45]. However, most of these works simply regard the solution space as a Euclidean space, where the underlying manifold structure and the equivariance priors of the task are ignored. One notable exception is [32], which developed an equivariant diffusion method for robotic manipulation, *i.e.*, pair-wise assembly tasks. Compared to [32], our method is conceptually simpler because it does not require Brownian diffusion on $SO(3)$ whose kernel is computationally intractable, and it solves the more general multi-piece problem. On the other hand, the invariant flow theory has been studied in [20], which can be regarded as a special case of our theory as discussed in Appx. C.1.

Another branch of related work is equivariant neural networks. Due to their ability to incorporate geometric priors, this type of networks has been widely used for processing 3D graph data such as PCs and molecules. In particular, E3NN [14] is a well-known equivariant network based on the tensor product of the input and the edge feature. An acceleration technique for E3NN was recently proposed [28]. On the other hand, the equivariant attention layer was studied in [12, 22, 24]. Our work is related to this line of approach, because our diffusion network can be seen as an equivariant network with an additional time parameter.

3 Preliminaries

This section introduces the major tools used in this work. We first define the equivariances in Sec. 3.1, then we briefly recall the flow matching model in Sec. 3.2.

3.1 Equivariances of PC assembly

Consider the action $G = \prod_{i=1}^{N} SE(3)$ on a set of N ($N \geq 2$) PCs $X = \{X_1, \dots, X_N\}$, where $SE(3)$ is the 3D rigid transformation group, $\prod$ is the direct product, and X_i is the i-th PC piece in 3D space. We define the action of $\boldsymbol{g} = (g_1, \dots, g_N) \in G$ on X as $\boldsymbol{g}X = \{g_i X_i\}_{i=1}^{N}$, *i.e.*, each PC X_i is rigidly transformed by the corresponding g_i. For the rotation subgroup $SO(3)^N$, the action of $\boldsymbol{r} = (r_1, \dots, r_N) \in SO(3)^N$ on X is $\boldsymbol{r}X = \{r_i X_i\}_{i=1}^{N}$. For $SO(3) \subseteq G$, we denote $r = (r, \dots, r) \in SO(3)$ for simplicity, and the action of r on X is written as $rX = \{rX_i\}_{i=1}^{N}$.

We also consider the permutation of X. Let S_N be the permutation group of N, the action of $\sigma \in S_N$ on X is $\sigma X = \{X_{\sigma(i)}\}_{i=1}^{N}$, and the action on $\boldsymbol{g}$ is $\sigma \boldsymbol{g} = (g_{\sigma(1)}, \dots, g_{\sigma(N)})$. For group multiplication, we denote $\mathcal{R}_{(\cdot)}$ the right multiplication and $\mathcal{L}_{(\cdot)}$ the left multiplication, *i.e.*, $(\mathcal{R}_{\boldsymbol{r}})\boldsymbol{r}' = \boldsymbol{r}'\boldsymbol{r}$, and $(\mathcal{L}_{\boldsymbol{r}})\boldsymbol{r}' = \boldsymbol{r}\boldsymbol{r}'$ for $\boldsymbol{r}, \boldsymbol{r}' \in SO(3)^N$.

In our setting, for the given input X, the solution to the assembly task is a conditional distribution $P_X \in \mu(G)$, where $\mu(G)$ is the set of probability distribution on G. We study the following three equivariances of P_X in this work:

Definition 3.1. Let $P_X \in \mu(G)$ be a probability distribution on $G = SE(3)^N$ conditioned on X, and let $(\cdot)_\#$ be the pushforward of measures.

- P_X is $SO(3)^N$-equivariant if $(\mathcal{R}_{\boldsymbol{r}^{-1}})_\# P_X = P_{\boldsymbol{r}X}$ for $\boldsymbol{r} \in SO(3)^N$.
- P_X is permutation-equivariant if $\sigma_\# P_X = P_{\sigma X}$ for $\sigma \in S_N$.
- P_X is $SO(3)$-invariant if $(\mathcal{L}_r)_\# P_X = P_X$ for $r \in SO(3)$.

Intuitively, the equivariances defined in Def. 3.1 are three natural priors of the assembly task: the $SO(3)^N$-equivariance of P_X implies that the solution will be properly transformed when X is rotated; the permutation-equivariance of P_X implies that the assembled shape is independent of the order of X; and the $SO(3)$-invariance of P_X implies that the solution does not have a preferred orientation.

Note that when $N = 2$, $SO(3)^N$-equivariance is closely related to $SE(3)$-bi-equivariance [32, 40], and permutation-equivariance becomes swap-equivariance in [40]. Detailed explanations can be found in Appx. B.

We finally recall the definition of $SO(3)$-equivariant networks, which will be the main computational tool of this work. We call $F^l \in \mathbb{R}^{2l+1}$ a degree-l $SO(3)$-equivariant feature if the action of $r \in SO(3)$ on F^l is the matrix-vector production: $rF^l = R^l F^l$, where $R^l \in \mathbb{R}^{(2l+1)\times(2l+1)}$ is the degree-l Wigner-D matrix of r. We call a network w $SO(3)$-equivariant if it maintains the equivariance from the input to the output: $w(rX) = rw(X)$, where $w(X)$ is a $SO(3)$-equivariant feature. More detailed introduction of equivariances and the underlying representation theory can be found in [3].

3.2 Vector fields and flow matching

To sample from a data distribution $P_1 \in \mu(M)$, where M is a smooth manifold (we only consider $M = G$ in this work), the flow matching [25] approach constructs a time-dependent diffeomorphism $\phi_\tau : M \to M$ satisfying $(\phi_0)_\# P_0 = P_0$ and $(\phi_1)_\# P_0 = P_1$, where $P_0 \in \mu(M)$ is a fixed noise distribution, and $\tau \in [0, 1]$ is the time parameter. Then the sample of P_1 can be represented as $\phi_1(g)$ where g is sampled from P_0.

Formally, ϕ_τ is defined as a flow, *i.e.*, an integral curve, generated by a time-dependent vector field $v_\tau : M \to TM$, where TM is the tangent bundle of M:

$$\begin{aligned} \frac{\partial}{\partial \tau}\phi_\tau(\boldsymbol{g}) &= v_\tau(\phi_\tau(\boldsymbol{g})), \\ \phi_0(\boldsymbol{g}) &= \boldsymbol{g}, \quad \forall \boldsymbol{g} \in M. \end{aligned} \tag{1}$$

According to [25], an efficient way to construct v_τ is to define a path h_τ connecting P_0 to P_1. Specifically, let $\boldsymbol{g}_0$ and $\boldsymbol{g}_1$ be samples from P_0 and P_1 respectively, and $h_0 = \boldsymbol{g}_0$ and $h_1 = \boldsymbol{g}_1$. v_τ can be constructed as the solution to the following problem:

$$\min_v \mathbb{E}_{\tau, \boldsymbol{g}_0 \sim P_0, \boldsymbol{g}_1 \sim P_1} ||v_\tau(h_\tau) - \frac{\partial}{\partial \tau} h_\tau||_F^2. \tag{2}$$

When v is learned using (2), we can obtain a sample from P_1 by first sampling a noise $\boldsymbol{g}_0$ from P_0 and then taking the integral of (1).

In this work, we consider a family of vector fields, flows and paths conditioned on the given PC, and we use the pushforward operator on vector fields to study their relatedness [37]. Formally, let $F : M \to M$ be a diffeomorphism, v and w be vector fields on M. w is F-related to v if $w(F(\boldsymbol{g})) = F_{*,\boldsymbol{g}} v(\boldsymbol{g})$ for all $\boldsymbol{g} \in M$, where $F_{*,\boldsymbol{g}}$ is the differential of F at $\boldsymbol{g}$. Note that we denote v_X, ϕ_X and h_X the vector field, flow and path conditioned on PC X respectively.

4 Method

In this section, we provide the details of the proposed Eda model. First, the PC assembly problem is formulated in Sec. 4.1. Then, we parametrize related vector fields in Sec. 4.2. The training and sampling procedures are finally described in Sec. 4.3 and Sec. 4.4 respectively.

4.1 Problem formulation

Given a set X containing N PC pieces, *i.e.*, $X = \{X_i\}_{i=1}^N$ where X_i is the i-th piece, the goal of assembly is to learn a distribution $P_X \in \mu(G)$, *i.e.*, for any sample $\boldsymbol{g}$ of P_X, $\boldsymbol{g}X$ should be the aligned complete shape. We assume that P_X has the following equivariances:

Assumption 4.1. P_X is $SO(3)^N$-equivariant, permutation-equivariant and $SO(3)$-invariant.

We seek to approximate P_X using flow matching. To avoid translation ambiguity, we also assume that, without loss of generality, the aligned PCs $\boldsymbol{g}X$ and each input piece X_i are centered, *i.e.*, $\sum_i \mathbf{m}(g_i X_i) = 0$, and $\mathbf{m}(X_i) = 0$ for all i, where $\mathbf{m}(\cdot)$ is the mean vector.

4.2 Equivariant flow

The major challenge in our task is to ensure the equivariance of the learned distribution, because a direct implement of flow matching (1) generally does not guarantee any equivariance. To address this challenge, we utilize the following theorem, which claims that when the noise distribution P_0 is invariant and vector fields v_X are related, the pushforward distribution $(\phi_X)\#P_0$ is guaranteed to be equivariant.

Theorem 4.2. *Let G be a smooth manifold, $F : G \to G$ be a diffeomorphism, and $P \in \mu(G)$. If vector field $v_X \in TG$ is F-related to vector field $v_Y \in TG$, then*

$$F_\# P_X = P_Y, \tag{3}$$

where $P_X = (\phi_X)_\# P_0$, $P_Y = (\phi_Y)_\#(F_\# P_0)$. Here $\phi_X, \phi_Y : G \to G$ are generated by v_X and v_Y respectively.

Specifically, Thm. 4.2 provides a concrete way to construct equivariant distributions as follow.

Assumption 4.3 (Invariant noise)**.** P_0 is $SO(3)^N$-invariant, permutation-invariant and $SO(3)$-invariant, *i.e.*, $(\mathcal{R}_{\boldsymbol{r}^{-1}})_\# P_0 = P_0$, $\sigma_\# P_0 = P_0$ and $P_0 = (\mathcal{L}_r)_\# P_0$ for $\boldsymbol{r} \in SO(3)^N$, $\sigma \in S_N$ and $r \in SO(3)$.

Corollary 4.4. *Under assumption 4.3,*

- *if v_X is $\mathcal{R}_{\boldsymbol{r}^{-1}}$-related to $v_{\boldsymbol{r}X}$, then $(\mathcal{R}_{\boldsymbol{r}^{-1}})_\# P_X = P_{\boldsymbol{r}X}$, where $P_X = (\phi_X)_\# P_0$ and $P_{\boldsymbol{r}X} = (\phi_{\boldsymbol{r}X})_\# P_0$. Here $\phi_X, \phi_{\boldsymbol{r}X} : G \to G$ are generated by v_X and $v_{\boldsymbol{r}X}$ respectively.*
- *if v_X is σ-related to $v_{\sigma X}$, then $\sigma_\# P_X = P_{\sigma X}$, where $P_X = (\phi_X)_\# P_0$ and $P_{\sigma X} = (\phi_{\sigma X})_\# P_0$. Here $\phi_X, \phi_{\sigma X} : G \to G$ are generated by v_X and $v_{\sigma X}$ respectively.*
- *if v_X is $\mathcal{L}_r$-invariant, i.e., v_X is $\mathcal{L}_r$-related to v_X, then $(\mathcal{L}_r)_\# P_X = P_X$, where $P_X = (\phi_X)_\# P_0$.*

Now we construct the vector field required by Cor. 4.4. We start by constructing $(\mathcal{R}_{\boldsymbol{g}^{-1}})$-related vector fields, which are $(\mathcal{R}_{\boldsymbol{r}^{-1}})$-related by definition, where $\boldsymbol{g} \in SE(3)^N$ and $\boldsymbol{r} \in SO(3)^N$. Specifically, we have the following proposition:

Proposition 4.5. *v_X is $\mathcal{R}_{\boldsymbol{g}^{-1}}$-related to $v_{\boldsymbol{g}X}$ if and only if $v_X(\boldsymbol{g}) = (\mathcal{R}_{\boldsymbol{g}})_{*,e} v_{\boldsymbol{g}X}(e)$ for all $\boldsymbol{g} \in SE(3)^N$.*

According to Prop. 4.5, to construct a $(\mathcal{R}_{\boldsymbol{g}^{-1}})$-related vector field v_X, we only need to parametrize v_X at the identity e. Specifically, let f be a neural network parametrizing $v_X(e)$, *i.e.*, $f(X) = v_X(e)$, we can define v_X as

$$v_X(\boldsymbol{g}) = (\mathcal{R}_{\boldsymbol{g}})_{*,e} f(\boldsymbol{g}X). \tag{4}$$

Here, $f(X) \in \mathfrak{se}(3)^N$ takes the form of

$$f(X) = \bigoplus_{i=1}^{N} f_i(X) \quad \text{where} \quad f_i(X) = \begin{pmatrix} w^i_\times(X) & t^i(X) \\ 0 & 0 \end{pmatrix} \in \mathfrak{se}(3) \subseteq \mathbb{R}^{4\times 4}. \tag{5}$$

The rotation component $w_\times^i(X) \in \mathbb{R}^{3\times 3}$ is a skew matrix with elements in the vector $w^i(X) \in \mathbb{R}^3$, and $t^i(X) \in \mathbb{R}^3$ is the translation component. For simplicity, we omit the superscript i when the context is clear.

Then we enforce the other two relatedness of v_X (4). According to the following proposition, σ-relatedness can be guaranteed if f is permutation-equivariant, and $\mathcal{L}_r$-invariance can be guaranteed if both w and t are SO(3)-equivariant.

Proposition 4.6. *For v_X defined in (4),*

- *if f is permutation-equivariant,* i.e., *$f(\sigma X) = \sigma f(X)$ for $\sigma \in S_N$ and PCs X, then $\sigma_\# v_X = v_{\sigma X}$;*
- *if f is SO(3)-equivariant,* i.e., *$w(rX) = rw(X)$ and $t(rX) = rt(X)$ for $r \in SO(3)$ and PCs X, then $(\mathcal{L}_r)_\# v_X = v_{rX}$.*

Finally, we define $P_0 = (U_{SO(3)} \otimes \mathcal{N}(0, \omega I))^N$, where $U_{SO(3)}$ is the uniform distribution on $SO(3)$, $\mathcal{N}$ is the normal distribution on $\mathbb{R}^3$ with mean zero and isotropic variance $\omega \in \mathbb{R}_+$, and $\otimes$ represents the independent coupling. It is straightforward to verify that P_0 indeed satisfies assumption 4.3.

In summary, with P_0 defined above and f (5) satisfying the assumptions in Prop. 4.6, Theorem 4.2 guarantees that the learned distribution has the desired equivariances, *i.e.*, $SO(3)^N$-equivariance, permutation-equivariance and $SO(3)$-invariance.

4.3 Training

To learn the vector field v_X (4) using flow matching (2), we now need to define h_X, and the sampling strategy of τ, $\boldsymbol{g}_0$ and $\boldsymbol{g}_1$. A canonical choice [4] is $h(\tau) = \boldsymbol{g}_0 \exp(\tau \log(\boldsymbol{g}_0^{-1}\boldsymbol{g}_1))$, where $\boldsymbol{g}_0$ and $\boldsymbol{g}_1$ are sampled independently, and τ is sampled from a predefined distribution, *e.g.*, the uniform distribution $U_{[0,1]}$. However, this definition of h, $\boldsymbol{g}_0$ and $\boldsymbol{g}_1$ does not utilize any equivariance property of v_X, thus it does not guarantee a high data efficiency.

To address this issue, we construct a "short" and equivariant h_X in the following two steps. First, we independently sample $\boldsymbol{g}_0$ from P_0 and $\tilde{\boldsymbol{g}}_1$ from P_X, and obtain $\boldsymbol{g}_1 = r^*\tilde{\boldsymbol{g}}_1$, where $r^* \in SO(3)$ is a rotation correction of $\tilde{\boldsymbol{g}}_1$:

$$r^* = \underset{r \in SO(3)}{\arg\min} ||r\tilde{\boldsymbol{g}}_1 - \boldsymbol{g}_0||_F^2. \tag{6}$$

Then, we define h_X as

$$h_X(\tau) = \exp(\tau \log(\boldsymbol{g}_1 \boldsymbol{g}_0^{-1}))\boldsymbol{g}_0. \tag{7}$$

We call h_X (7) a path generated by $\boldsymbol{g}_0$ and $\tilde{\boldsymbol{g}}_1$. Note that h_X (7) is a well-defined path connecting $\boldsymbol{g}_0$ to $\boldsymbol{g}_1$, because $h_X(0) = \boldsymbol{g}_0$ and $h_X(1) = \boldsymbol{g}_1$, and $\boldsymbol{g}_1$ follows P_X (Prop. C.5).

The advantages of h_X (7) are twofold. First, instead of connecting a noise $\boldsymbol{g}_0$ to an independent data sample $\tilde{\boldsymbol{g}}_1$, h_X connects $\boldsymbol{g}_0$ to a modified sample $\boldsymbol{g}_1$ where the redundant rotation component is removed, thus it is easier to learn. Second, the velocity fields of h_X enjoy the same relatedness as v_X (4), which leads to high data efficiency. Formally, we have the following observation.

Proposition 4.7 (Data efficiency)**.** *Under assumption 4.3, 4.1, and C.4, we further assume that v_X satisfies the relatedness property required in Cor. 4.4,* i.e., *v_X is $\mathcal{R}_{\boldsymbol{r}^{-1}}$-related to $v_{\boldsymbol{r}X}$, v_X is σ-related to $v_{\sigma X}$, and v_X is $\mathcal{L}_r$-invariant. Denote $L(X) = \mathbb{E}_{\tau, \boldsymbol{g}_0 \sim P_0, \tilde{\boldsymbol{g}}_1 \sim P_X} ||v_X(h_X(\tau)) - \frac{\partial}{\partial \tau} h_X(\tau)||_F^2$ the training loss (2) of PC X, where h_X is generated by $\boldsymbol{g}_0$ and $\tilde{\boldsymbol{g}}_1$ as defined in (7). Then*

- *$L(X) = L(\boldsymbol{r}X)$ for $\boldsymbol{r} \in SO(3)^N$.*
- *$L(X) = L(\sigma X)$ for $\sigma \in S_N$.*
- *$L(X) = \hat{L}(X)$, where $\hat{L}(X) = \mathbb{E}_{\tau, \boldsymbol{g}_0' \sim P_0, \tilde{\boldsymbol{g}}_1' \sim (\mathcal{L}_r)_\# P_X} ||v_X(h_X(\tau)) - \frac{\partial}{\partial \tau} h_X(\tau)||_F^2$ is the loss where the data distribution P_X is pushed forward by $\mathcal{L}_r \in SO(3)$.*

Prop. 4.7 implies that when h_X (7) is combined with the equivariant components developed in Sec. 4.2, the following three data augmentations are not needed: 1) random rotation of each input piece X_i, 2) random permutation of the order of the input pieces, and 3) random rotation of the assembled shape, because they have no influence on the training loss.

4.4 Sampling via the Runge-Kutta method

Finally, when the vector field v_X (4) is learned, we can obtain a sample $\boldsymbol{g}_1$ from P_X by numerically integrating v_X starting from a noise $\boldsymbol{g}_0$ from P_0. In this work, we use the Runge-Kutta (RK) solver on $SE(3)^N$, which is a generalization of the classical RK solver on Euclidean spaces. For clarity, we present the formulations below, and refer the readers to [7] for more details.

To apply the RK method, we first discretize the time interval $[0, 1]$ into I steps, *i.e.*, $\tau_i = \frac{i}{I}$ for $i = 0, \dots, I$, with a step length $\eta = \frac{1}{I}$. For the given input X, denote $f(\boldsymbol{g}X)$ at time τ by $f_\tau(\boldsymbol{g})$ for simplicity. The first-order RK method (RK1), *i.e.*, the Euler method, is to iterate:

$$\boldsymbol{g}_{i+1} = \exp(\eta f_{\tau_i}(\boldsymbol{g}_i))\boldsymbol{g}_i, \tag{8}$$

for $i = 0, \dots, I$. To achieve higher accuracy, we can use the fourth-order RK method (RK4):

$$k_1 = f_{\tau_i}(\boldsymbol{g}_i),\ k_2 = f_{\tau_i+\frac{1}{2}\eta}\big(\exp(\frac{1}{2}\eta k_1)\boldsymbol{g}_i\big),\ k_3 = f_{\tau_i+\frac{1}{2}\eta}\big(\exp(\frac{1}{2}\eta k_2)\boldsymbol{g}_i\big),\ k_4 = f_{\tau_i+\eta}\big(\exp(\eta k_3)\boldsymbol{g}_i\big),$$
$$\boldsymbol{g}_{i+1} = \exp(\frac{1}{6}\eta k_4)\exp(\frac{1}{3}\eta k_3)\exp(\frac{1}{3}\eta k_2)\exp(\frac{1}{6}\eta k_1)\boldsymbol{g}_i. \tag{9}$$

Note that RK4 (9) is more computationally expensive than RK1 (8), because it requires four evaluations of v_X at different points at each step, *i.e.*, four forward passes of network f, while the Euler method only requires one evaluation per step.

5 Implementation

This section provides the details of the network f (5). Our design principle is to imitate the standard transformer structure [38] to retain its best practices. In addition, according to Prop. 4.6, we also require f to be permutation-equivariant and $SO(3)$-equivariant.

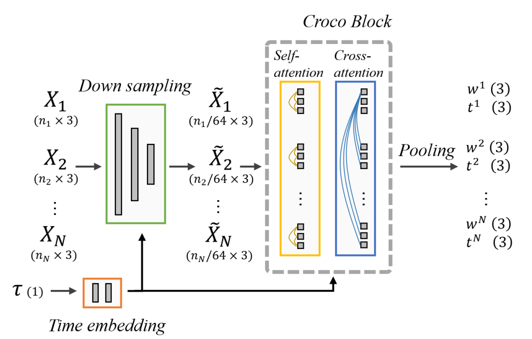

Figure 1: An overview of our model. The shapes of variables are shown in the brackets.

The overall structure of the proposed network is shown in Fig. 1. In a forward pass, the input PC pieces $\{X_i\}_{i=1}^N$ are first downsampled using a few downsampling blocks, and then fed into the Croco blocks [42] to model their relations. Meanwhile, the time step τ is first embedded using a multi-layer perceptron (MLP) and then incorporated into the above blocks via adaptive normalization [29]. The output is finally obtained by a piece-wise pooling.

Next, we provide details of the equivariant attention layers, which are the major components of both the downsampling block and the Croco block, in Sec. 5.1. Other layers, including the nonlinear and normalization layers, are described in Sec. 5.2.

5.1 Equivariant attention layers

Let $F_u^l \in \mathbb{R}^{c\times(2l+1)}$ be a channel-c degree-l feature at point u. The equivariant dot-product attention is defined as:

$$A_u^l = \sum_{v\in \mathit{KNN}(u)\setminus\{u\}} \frac{\exp\left(\langle Q_u, K_{vu}\rangle\right)}{\sum_{v'\in \mathit{KNN}(u)\setminus\{u\}}\exp\left(\langle Q_u, K_{v'u}\rangle\right)} V_{vu}^l, \tag{10}$$

where $\langle\cdot,\cdot\rangle$ is the dot product, $\mathit{KNN}(u) \subseteq \bigcup_i X_i$ is a subset of points u attends to, $K, V \in \mathbb{R}^{c\times(2l+1)}$ take the form of the e3nn [14] message passing, and $Q \in \mathbb{R}^{c\times(2l+1)}$ is obtained by a linear transform:

$$Q_u = \bigoplus_l W_Q^l F_u^l, \quad K_v = \bigoplus_l \sum_{l_e, l_f} c_K^{(l,l_e,l_f)}(|uv|)Y^{l_e}(\widehat{vu}) \otimes_{l_e,l_f}^l F_v^{l_f}, \tag{11}$$

$$V_v^l = \sum_{l_e,l_f} c_V^{(l,l_e,l_f)}(|uv|)Y^{l_e}(\widehat{vu}) \otimes_{l_e,l_f}^l F_v^{l_f}. \tag{12}$$

Here, $W_Q^l \in \mathbb{R}^{c \times c}$ is a learnable weight, $|vu|$ is the distance between point v and u, $\widehat{vu} = \vec{vu}/|vu| \in \mathbb{R}^3$ is the normalized direction, $Y^l : \mathbb{R}^3 \to \mathbb{R}^{2l+1}$ is the degree-l spherical harmonic function, $c : \mathbb{R}_+ \to \mathbb{R}$ is a learnable function that maps $|vu|$ to a coefficient, and $\otimes$ is the tensor product with the Clebsch-Gordan coefficients.

To accelerate the computation of K and V, we use the $SO(2)$-reduction technique [28], which rotates the edge uv to the y-axis, so that the computation of spherical harmonic function, the Clebsch-Gordan coefficients, and the iterations of l_e are no longer needed. More details are provided in Appx. D.

Following Croco [42], we stack two types of attention layers, *i.e.*, the self-attention layer and the cross-attention layer, into a Croco block to learn the features of each PC piece while incorporating information from other pieces. For self-attention layers, we set $KNN(u)$ to be the k-nearest neighbors of u in the same piece, and for cross-attention layers, we set $KNN(u)$ to be the k-nearest neighbors of u in each of the different pieces. In addition, to reduce the computational cost, we use downsampling layers to reduce the number of points before the Croco layers. Each downsampling layer consists of a farthest point sampling (FPS) layer and a self-attention layer.

5.2 Adaptive normalization and nonlinear layers

Following the common practice [10], we seek to use the GELU activation function [16] in our transformer structure. However, GELU in its original form is not $SO(3)$-equivariant. To address this issue, we adopt a projection formulation similar to [9]. Specifically, we define the equivariant GELU (Elu) as:

$$\mathit{Elu}(F^l) = \mathit{GELU}(\langle F^l, \widehat{WF^l} \rangle) \tag{13}$$

where $\widehat{x} = x/\|x\|$ is the normalized feature, $W \in \mathbb{R}^{c \times c}$ is a learnable weight. Note that Elu (13) is a natural extension of GELU, because when $l = 0$, $\mathit{Elu}(F^0) = \mathit{GELU}(\pm F^0)$.

As for the normalization layers, we use RMS-type layer normalization layers [50] following [23], and we use the adaptive normalization [29] technique to incorporate the time step τ. Specifically, we use the adaptive normalization layer *AN* defined as:

$$\mathit{AN}(F^l, \tau) = F^l/\sigma \cdot \mathit{MLP}(\tau), \tag{14}$$

where $\sigma = \sqrt{\frac{1}{c \cdot l_{max}} \sum_{l=1}^{l_{max}} \frac{1}{2l+1} \langle F^l, F^l \rangle}$, l_{max} is the maximum degree, and *MLP* is a multi-layer perceptron that maps τ to a vector of length c.

We finally remark that the network $\boldsymbol{f}$ defined in this section is $SO(3)$-equivariant because each layer is $SO(3)$-equivariant by construction. $\boldsymbol{f}$ is also permutation-equivariant because it does not use any order information of X_i.

6 Experiment

This section evaluates Eda on practical assembly tasks. After introducing the experiment settings in Sec. 6.1, we first evaluate Eda on the pair-wise registration tasks in Sec. 6.2, and then we consider the multi-piece assembly tasks in Sec. 6.3. An ablation study on the number of PC pieces is finally presented in Sec. 6.4.

6.1 Experiment settings

We evaluate the accuracy of an assembly solution using the averaged pair-wise error. For a predicted assembly $\boldsymbol{g}$ and the ground truth $\hat{\boldsymbol{g}}$, the rotation error Δr and the translation error Δt are computed as: $(\Delta r, \Delta t) = \frac{1}{N(N-1)} \sum_{i \neq j} \tilde{\Delta}(\hat{g}_i, \hat{g}_j g_j^{-1} g_i)$, where the pair-wise error $\tilde{\Delta}$ is computed as $\tilde{\Delta}(g, \hat{g}) = \left(\frac{180}{\pi} \mathit{accos}\left(\frac{1}{2} \left(\mathit{tr}(r\hat{r}^T) - 1 \right) \right), \|\hat{t} - t\| \right)$. Here $g = (r, t)$, $\hat{g} = (\hat{r}, \hat{t})$, and $\mathit{tr}(\cdot)$ represents the trace.

For Eda, we use 2 Croco blocks, and 4 downsampling layers with a downsampling ratio 0.25. We use $k = 10$ nearest neighbors, $l_{max} = 2$ degree features with $d = 64$ channels and 4 attention heads. Following [29], we keep an exponential moving average (EMA) with a decay of 0.99, and we use the AdamW [26] optimizer with a learning rate 10^{-4}. Following [11], we use a logit-normal sampling for time variable τ. For each experiment, we train Eda on 3 Nvidia A100 GPUs for at most 5 days. We denote Eda with q steps of RKp as "Eda (RKp, q)" , *e.g.*, Eda (RK1, 10) represents Eda with 10 steps of RK1.

6.2 Pair-wise registration

This section evaluates Eda on rotated 3DMatch [48] (3DM) dataset containing PC pairs from indoor scenes. Following [17], we consider the 3DLoMatch split (3DL), which contains PC pairs with smaller overlap ratios. Furthermore, to highlight the ability of Eda on non-overlapped assembly tasks, we consider a new split called 3DZeroMatch (3DZ), which contains non-overlapped PC pairs. The comparison of these three splits is shown in Tab. 1.

Table 1: The overlap ratio of PC pairs (%).

	3DM	3DL	3DZ
Training set	$(10, 100)$		0
Test set	$(30, 100)$	$(10, 30)$	0

We compare Eda against the following baseline methods: FGR [52], GEO [30], ROI [47], and AMR [6], where FGR is a classic optimization-based method, GEO and ROI are correspondence-based methods, and AMR is a recently proposed diffusion-like method based on GEO. We report the results of the baseline methods using their official implementations. Note that the correspondence-free methods like [32, 40] do not scale to this dataset.

Table 2: Quantitative results on rotated 3DMatch. ROI (n): ROI with n RANSAC samples.

	3DM		3DL		3DZ	
	Δr	Δt	Δr	Δt	Δr	Δt
FGR	69.5	0.6	117.3	1.3	–	–
GEO	7.43	0.19	28.38	0.69	–	–
ROI (500)	5.64	0.15	21.94	0.53	–	–
ROI (5000)	5.44	0.15	22.17	0.53	–	–
AMR	5.0	**0.13**	20.5	0.53	–	–
Eda (RK4, 50)	**2.38**	0.17	**8.57**	**0.4**	78.32	2.74

We report the results in Tab 2. On 3DM and 3DL, we observe that Eda outperforms the baseline methods by a large margin, especially for rotation errors, where Eda achieves more than 50% lower rotation errors on both 3DL and 3DM. We provide more details of Eda on 3DL in Fig. 5 in the appendix.

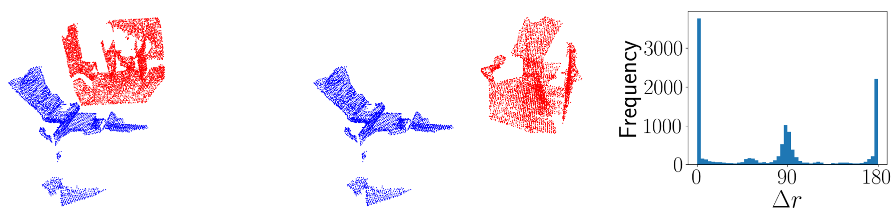

(a) The result of Eda (b) Ground truth (c) Distribution of Δr

Figure 2: More details of Eda on 3DZ. A result of Eda is shown in (a) ($\Delta r = 90.2$). Two PC pieces are marked by different colors. Δr is centered at 0, 90, and 180 on the test set (c), suggesting that Eda learns to keeps the orthogonality or parallelism of walls, floors and ceilings of the indoor scenes.

As for 3DZ, we only report the results of Eda in Tab 2, because all baseline methods are not applicable to 3DZ, *i.e.*, their training goal is undefined when the correspondence does not exist. We observe that Eda's error on 3DZ is much larger compared to that on 3DL, suggesting that there exists much larger ambiguity. We provide an example of the result of Eda in Fig. 2. One important observation is that despite the ambiguity of the data, Eda learned the global geometry of the indoor scenes, in the sense that it tends to place large planes, *i.e.*, walls, floors and ceilings, in a parallel or orthogonal position.

To show that this behavior is consistent in the whole test set, we present the distribution of Δr of Eda on 3DZ in Fig. 2(c). A simple intuition is that for rooms consisting of 6 parallel or orthogonal planes (four walls, a floor and a ceiling), if the orthogonality or parallelism of planes is correctly maintained in the assembly, then Δr should be 0, 90, or 180. We observe that this is indeed the case in Fig. 2(c), where Δr is centered at 0, 90, and 180. We remark that the ability to learn global geometric properties beyond correspondences is a key advantage of Eda, and it partially explains the superior performance of Eda in Tab. 2

6.3 Multi-piece assembly

This section evaluates Eda on the volume constrained version of BB dataset [35]. We consider the shapes with $2 \leq N \leq 8$ pieces in the "everyday" subset. We compare Eda against the following baseline methods: DGL [49], LEV [43], GLO [35] and JIG [27]. JIG is correspondence-based, and other baseline methods are regression-based. Note that we do not report the results of the diffusion-type method [34] due to accessibility issues. We process all fragments by grid downsampling with a grid size 0.02 for Eda. For the baseline methods, we follow their original preprocessing steps. To reproduce the results of the baseline methods, we use the implement of DGL and GLO in the official benchmark suite of BB, and we use the official implement of LEV and JIG.

The results are shown in Tab. 3, where we also report the computation time for the whole test set containing 6904 shapes on a Nvidia T4 GPU. We observe that Eda outperforms all baseline methods by a large margin at a moderate computation cost. We present some qualitative results from Fig. 6 to 8 in the appendix, where we observe that Eda can generally reconstruct the shapes more accurately than the baseline methods. An example of the assembly process of Eda is presented in Fig. 3.

Table 3: Quantitative results on BB dataset and the total computation time on the test set.

	Δr	Δt	Time (min)
GLO	126.3	0.3	**0.9**
DGL	125.8	0.3	**0.9**
LEV	125.9	0.3	8.1
JIG	106.5	0.24	122.2
Eda (RK1, 10)	80.64	**0.16**	19.4
Eda (RK4, 10)	**79.2**	**0.16**	76.9

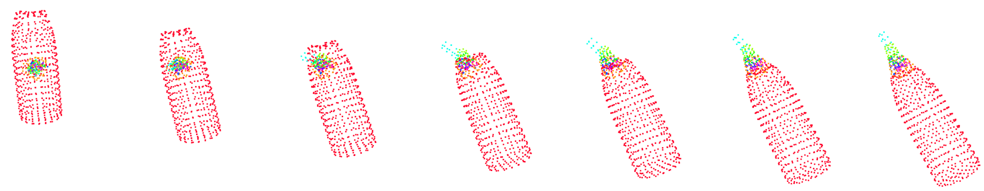

Figure 3: From left to right: the assembly process of a 8-piece bottle by Eda.

6.4 Ablation on the number of pieces

This section investigates the influence of the number of pieces on the performance of Eda. We use the kitti odometry dataset [13] containing PCs of city road views. For each sequence of data, we keep pieces that are at least 100 meters apart so that they do not necessarily overlap, and we downsample them using grid downsampling with a grid size 0.5. We train Eda on all consecutive pieces of length $2 \sim N_{max}$ in sequences $0 \sim 8$. We call the trained model Eda-N_{max}. We then evaluate Eda-N_{max} on all consecutive pieces of length M in sequence $9 \sim 10$.

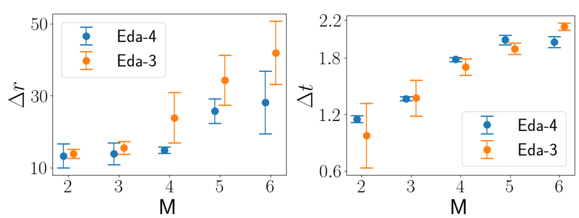

Figure 4: The results of Eda on different number of pieces.

The results are shown in Fig. 4. We observe that for Δr, when the length of the test data is seen in the training set, *i.e.*, $M \leq N_{max}$, Eda performs well, and $M > N_{max}$ leads to worse performance. In addition, Eda-4 generalizes better than Eda-3 on data of unseen length (5 and 6). The result indicates the necessity of using training data of similar length to the test data. Meanwhile, the translation errors of Eda-4 and Eda-3 are comparable, and they both increase with the length of test data.

7 Conclusion and discussion

This work studied the theory of equivariant flow matching, and presented a multi-piece assembly method, called Eda, based on the theory. We show that Eda can accurately assemble PCs on practical datasets.

Eda in its current form has several limitations. First, Eda is slow when using a high order RK solver with a large number of steps. Besides its iterative nature, another cause is the lack of kernel level optimization like FlashAttention [8] for equivariant attention layers. We expect to see acceleration in the future when such optimization is available. Second, Eda always uses all input pieces, which is not suitable for applications like archeology reconstruction, where the input data may contain pieces from unrelated objects. Finally, we have not studied the scaling law [19] of Eda in this work, where we expect to see that an increase in model size leads to an increase in performance similar to image generation applications [29].

References

[1] Federica Arrigoni, Beatrice Rossi, and Andrea Fusiello. Spectral synchronization of multiple views in se (3). *SIAM Journal on Imaging Sciences*, 9(4):1963–1990, 2016.

[2] K Somani Arun, Thomas S Huang, and Steven D Blostein. Least-squares fitting of two 3-d point sets. *IEEE Transactions on pattern analysis and machine intelligence*, (5):698–700, 1987.

[3] Gabriele Cesa, Leon Lang, and Maurice Weiler. A program to build e (n)-equivariant steerable cnns. In *International Conference on Learning Representations*, 2022.

[4] Ricky TQ Chen and Yaron Lipman. Flow matching on general geometries. In *The Twelfth International Conference on Learning Representations*, 2024.

[5] Yun-Chun Chen, Haoda Li, Dylan Turpin, Alec Jacobson, and Animesh Garg. Neural shape mating: Self-supervised object assembly with adversarial shape priors. In *Proceedings of the IEEE/CVF Conference on Computer Vision and Pattern Recognition*, pages 12724–12733, 2022.

[6] Zhi Chen, Yufan Ren, Tong Zhang, Zheng Dang, Wenbing Tao, Sabine Susstrunk, and Mathieu Salzmann. Adaptive multi-step refinement network for robust point cloud registration. *Transactions on Machine Learning Research*, 2025.

[7] Peter E Crouch and R Grossman. Numerical integration of ordinary differential equations on manifolds. *Journal of Nonlinear Science*, 3:1–33, 1993.

[8] Tri Dao, Daniel Y. Fu, Stefano Ermon, Atri Rudra, and Christopher Ré. FlashAttention: Fast and memory-efficient exact attention with IO-awareness. In *Advances in Neural Information Processing Systems (NeurIPS)*, 2022.

[9] Congyue Deng, Or Litany, Yueqi Duan, Adrien Poulenard, Andrea Tagliasacchi, and Leonidas J Guibas. Vector neurons: A general framework for so (3)-equivariant networks. In *Proceedings of the IEEE/CVF International Conference on Computer Vision*, pages 12200–12209, 2021.

[10] Jacob Devlin, Ming-Wei Chang, Kenton Lee, and Kristina Toutanova. Bert: Pre-training of deep bidirectional transformers for language understanding. In *Proceedings of the 2019 conference of the North American chapter of the association for computational linguistics: human language technologies, volume 1 (long and short papers)*, pages 4171–4186, 2019.

[11] Patrick Esser, Sumith Kulal, Andreas Blattmann, Rahim Entezari, Jonas Müller, Harry Saini, Yam Levi, Dominik Lorenz, Axel Sauer, Frederic Boesel, et al. Scaling rectified flow transformers for high-resolution image synthesis. In *Forty-first international conference on machine learning*, 2024.

[12] Fabian Fuchs, Daniel Worrall, Volker Fischer, and Max Welling. Se(3)-transformers: 3d roto-translation equivariant attention networks. *Advances in neural information processing systems*, 33:1970–1981, 2020.

[13] Andreas Geiger, Philip Lenz, and Raquel Urtasun. Are we ready for autonomous driving? the kitti vision benchmark suite. In *2012 IEEE conference on computer vision and pattern recognition*, pages 3354–3361. IEEE, 2012.

[14] Mario Geiger and Tess Smidt. e3nn: Euclidean neural networks. *arXiv preprint arXiv:2207.09453*, 2022.

[15] Zan Gojcic, Caifa Zhou, Jan D Wegner, Leonidas J Guibas, and Tolga Birdal. Learning multiview 3d point cloud registration. In *International conference on computer vision and pattern recognition (CVPR)*, 2020.

[16] Dan Hendrycks and Kevin Gimpel. Gaussian error linear units (gelus). *arXiv preprint arXiv:1606.08415*, 2016.

[17] Shengyu Huang, Zan Gojcic, Mikhail Usvyatsov, Andreas Wieser, and Konrad Schindler. Predator: Registration of 3d point clouds with low overlap. In *Proceedings of the IEEE/CVF Conference on computer vision and pattern recognition*, pages 4267–4276, 2021.

[18] Haobo Jiang, Mathieu Salzmann, Zheng Dang, Jin Xie, and Jian Yang. Se (3) diffusion model-based point cloud registration for robust 6d object pose estimation. *Advances in Neural Information Processing Systems*, 36:21285–21297, 2023.

[19] Jared Kaplan, Sam McCandlish, Tom Henighan, Tom B Brown, Benjamin Chess, Rewon Child, Scott Gray, Alec Radford, Jeffrey Wu, and Dario Amodei. Scaling laws for neural language models. *arXiv preprint arXiv:2001.08361*, 2020.

[20] Jonas Köhler, Leon Klein, and Frank Noé. Equivariant flows: exact likelihood generative learning for symmetric densities. In *International conference on machine learning*, pages 5361–5370. PMLR, 2020.

[21] Seong Hun Lee and Javier Civera. Hara: A hierarchical approach for robust rotation averaging. In *Proceedings of the IEEE/CVF Conference on Computer Vision and Pattern Recognition*, pages 15777–15786, 2022.

[22] Yi-Lun Liao and Tess Smidt. Equiformer: Equivariant graph attention transformer for 3d atomistic graphs. In *The Eleventh International Conference on Learning Representations*, 2023.

[23] Yi-Lun Liao, Brandon Wood, Abhishek Das, and Tess Smidt. Equiformerv2: Improved equivariant transformer for scaling to higher-degree representations. *arXiv preprint arXiv:2306.12059*, 2023.

[24] Yi-Lun Liao, Brandon M Wood, Abhishek Das, and Tess Smidt. Equiformerv2: Improved equivariant transformer for scaling to higher-degree representations. In *The Twelfth International Conference on Learning Representations*, 2024.

[25] Yaron Lipman, Ricky T. Q. Chen, Heli Ben-Hamu, Maximilian Nickel, and Matthew Le. Flow matching for generative modeling. In *The Eleventh International Conference on Learning Representations*, 2023.

[26] Ilya Loshchilov and Frank Hutter. Decoupled weight decay regularization. *arXiv preprint arXiv:1711.05101*, 2017.

[27] Jiaxin Lu, Yifan Sun, and Qixing Huang. Jigsaw: Learning to assemble multiple fractured objects. *Advances in Neural Information Processing Systems*, 36:14969–14986, 2023.

[28] Saro Passaro and C Lawrence Zitnick. Reducing so (3) convolutions to so (2) for efficient equivariant gnns. In *International Conference on Machine Learning*, pages 27420–27438. PMLR, 2023.

[29] William Peebles and Saining Xie. Scalable diffusion models with transformers. In *Proceedings of the IEEE/CVF international conference on computer vision*, pages 4195–4205, 2023.

[30] Zheng Qin, Hao Yu, Changjian Wang, Yulan Guo, Yuxing Peng, and Kai Xu. Geometric transformer for fast and robust point cloud registration. In *Proceedings of the IEEE/CVF conference on computer vision and pattern recognition*, pages 11143–11152, 2022.

[31] Hyunwoo Ryu, Hong in Lee, Jeong-Hoon Lee, and Jongeun Choi. Equivariant descriptor fields: Se(3)-equivariant energy-based models for end-to-end visual robotic manipulation learning. In *The Eleventh International Conference on Learning Representations*, 2023.

[32] Hyunwoo Ryu, Jiwoo Kim, Hyunseok An, Junwoo Chang, Joohwan Seo, Taehan Kim, Yubin Kim, Chaewon Hwang, Jongeun Choi, and Roberto Horowitz. Diffusion-edfs: Bi-equivariant denoising generative modeling on se (3) for visual robotic manipulation. In *Proceedings of the IEEE/CVF Conference on Computer Vision and Pattern Recognition*, pages 18007–18018, 2024.

[33] Hyunwoo Ryu, Hong-in Lee, Jeong-Hoon Lee, and Jongeun Choi. Equivariant descriptor fields: Se (3)-equivariant energy-based models for end-to-end visual robotic manipulation learning. *arXiv preprint arXiv:2206.08321*, 2022.

[34] Gianluca Scarpellini, Stefano Fiorini, Francesco Giuliari, Pietro Moreiro, and Alessio Del Bue. Diffassemble: A unified graph-diffusion model for 2d and 3d reassembly. In *Proceedings of the IEEE/CVF Conference on Computer Vision and Pattern Recognition*, pages 28098–28108, 2024.

[35] Silvia Sellán, Yun-Chun Chen, Ziyi Wu, Animesh Garg, and Alec Jacobson. Breaking bad: A dataset for geometric fracture and reassembly. *Advances in Neural Information Processing Systems*, 35:38885–38898, 2022.

[36] Anthony Simeonov, Yilun Du, Andrea Tagliasacchi, Joshua B Tenenbaum, Alberto Rodriguez, Pulkit Agrawal, and Vincent Sitzmann. Neural descriptor fields: Se (3)-equivariant object representations for manipulation. In *2022 International Conference on Robotics and Automation (ICRA)*, pages 6394–6400. IEEE, 2022.

[37] Loring W Tu. Manifolds. In *An Introduction to Manifolds*, pages 47–83. Springer, 2011.

[38] Ashish Vaswani, Noam Shazeer, Niki Parmar, Jakob Uszkoreit, Llion Jones, Aidan N Gomez, Łukasz Kaiser, and Illia Polosukhin. Attention is all you need. *Advances in neural information processing systems*, 30, 2017.

[39] Haiping Wang, Yufu Zang, Fuxun Liang, Zhen Dong, Hongchao Fan, and Bisheng Yang. A probabilistic method for fractured cultural relics automatic reassembly. *Journal on Computing and Cultural Heritage (JOCCH)*, 14(1):1–25, 2021.

[40] Ziming Wang and Rebecka Jörnsten. Se (3)-bi-equivariant transformers for point cloud assembly. In *The Thirty-eighth Annual Conference on Neural Information Processing Systems (NeurIPS)*, 2024.

[41] Joseph L Watson, David Juergens, Nathaniel R Bennett, Brian L Trippe, Jason Yim, Helen E Eisenach, Woody Ahern, Andrew J Borst, Robert J Ragotte, Lukas F Milles, et al. De novo design of protein structure and function with rfdiffusion. *Nature*, 620(7976):1089–1100, 2023.

[42] Philippe Weinzaepfel, Vincent Leroy, Thomas Lucas, Romain Brégier, Yohann Cabon, Vaibhav Arora, Leonid Antsfeld, Boris Chidlovskii, Gabriela Csurka, and Jérôme Revaud. Croco: Self-supervised pre-training for 3d vision tasks by cross-view completion. *Advances in Neural Information Processing Systems*, 35:3502–3516, 2022.

[43] Ruihai Wu, Chenrui Tie, Yushi Du, Yan Zhao, and Hao Dong. Leveraging se (3) equivariance for learning 3d geometric shape assembly. In *Proceedings of the IEEE/CVF International Conference on Computer Vision*, pages 14311–14320, 2023.

[44] Yue Wu, Yongzhe Yuan, Xiaolong Fan, Xiaoshui Huang, Maoguo Gong, and Qiguang Miao. Pcrdiffusion: Diffusion probabilistic models for point cloud registration. *CoRR*, 2023.

[45] Qun-Ce Xu, Hao-Xiang Chen, Jiacheng Hua, Xiaohua Zhan, Yong-Liang Yang, and Tai-Jiang Mu. Fragmentdiff: A diffusion model for fractured object assembly. In *SIGGRAPH Asia 2024 Conference Papers*, pages 1–12, 2024.

[46] Jason Yim, Andrew Campbell, Andrew YK Foong, Michael Gastegger, José Jiménez-Luna, Sarah Lewis, Victor Garcia Satorras, Bastiaan S Veeling, Regina Barzilay, Tommi Jaakkola, et al. Fast protein backbone generation with se (3) flow matching. *arXiv preprint arXiv:2310.05297*, 2023.

[47] Hao Yu, Zheng Qin, Ji Hou, Mahdi Saleh, Dongsheng Li, Benjamin Busam, and Slobodan Ilic. Rotation-invariant transformer for point cloud matching. In *Proceedings of the IEEE/CVF conference on computer vision and pattern recognition*, pages 5384–5393, 2023.

[48] Andy Zeng, Shuran Song, Matthias Nießner, Matthew Fisher, Jianxiong Xiao, and Thomas Funkhouser. 3dmatch: Learning local geometric descriptors from rgb-d reconstructions. In *Proceedings of the IEEE conference on computer vision and pattern recognition*, pages 1802–1811, 2017.

[49] Guanqi Zhan, Qingnan Fan, Kaichun Mo, Lin Shao, Baoquan Chen, Leonidas J Guibas, Hao Dong, et al. Generative 3d part assembly via dynamic graph learning. *Advances in Neural Information Processing Systems*, 33:6315–6326, 2020.

[50] Biao Zhang and Rico Sennrich. Root mean square layer normalization. *Advances in Neural Information Processing Systems*, 32, 2019.

[51] Zhengyou Zhang. Iterative point matching for registration of free-form curves and surfaces. *International Journal of Computer Vision*, 13(2):119–152, 1994.

[52] Qian-Yi Zhou, Jaesik Park, and Vladlen Koltun. Fast global registration. In *Computer Vision–ECCV 2016: 14th European Conference, Amsterdam, The Netherlands, October 11-14, 2016, Proceedings, Part II 14*, pages 766–782. Springer, 2016.

A More details of the related tasks

The registration task aims to reconstruct the scene from multiple overlapped views. A registration method generally consists of two stages: first, each pair of pieces is aligned using a pair-wise method [30], then all pieces are merged into a complete shape using a synchronization method [1, 21, 15]. In contrast to other tasks, the registration task generally assumes that the pieces are overlapped. In other words, it assumes that some points observed in one piece are also observed in the other piece, and the goal is to match the points observed in both pieces, *i.e.*, corresponding points. The state-of-the-art registration methods usually infer the correspondences based on the feature similarity [47] learned by neural networks, and then align them using the SVD projection [2] or RANSAC.

The robotic manipulation task aims to move one PC to a certain position relative to another PC. For example, one PC can be a cup, and the other PC can be a table, and the goal is to move the cup on the table. Since the input PCs are sampled from different objects, they are generally non-overlapped. Unlike the other two tasks, this task is generally formulated in a probabilistic setting, as the solution is generally not unique. Various probabilistic models, such as energy based model [36, 31], or diffusion model [32], have been used for this task.

The reassembly task aims to reconstruct the complete object from multiple fragment pieces. This task is similar to the registration task, except that the input PCs are sampled from different fragments, thus they are not necessarily overlapped, *e.g.*, due to missing pieces or the erosion of the surfaces. Most of the existing methods are based on regression, where the solution is directly predicted from the input PCs [43, 5, 40]. Some probabilistic methods, such as diffusion based methods [45, 34], have also been proposed. Note that there exist some exceptions [27] which assume the overlap of the pieces, and they reply on the inferred correspondences as the registration methods.

A comparison of these three tasks is presented in Tab. 4.

Table 4: Comparison between registration, reassembly and manipulation tasks.

Task	Number of pieces	Probabilistic/Deterministic	Overlap
Registration	2 [30] or more [15]	Deterministic	Overlapped
Reassembly	≥ 2	Deterministic	Non-overlapped
Manipulation	2	Probabilistic	Non-overlapped
Assembly (this work)	≥ 2	Probabilistic	Non-overlapped

B Connections with bi-equivariance

This section briefly discusses the connections between Def. 3.1 and the equivariances defined in [32] and [40] in pair-wise assembly tasks.

We first recall the definition of the probabilistic bi-equivariance.

Definition B.1 (Eqn. (10) in [32] and Def. (1) in [33])**.** $\hat{P} \in \mu(SE(3))$ is bi-equivariant if for all $g_1, g_2 \in SO(3)$, PCs X_1, X_2, and measurable set $A \subseteq SE(3)$,

$$\hat{P}(A|X_1, X_2) = \hat{P}(g_2 A g_1^{-1}|g_1 X_1, g_2 X_2). \tag{15}$$

Note that we only consider $g_1, g_2 \in SO(3)$ instead of $g_1, g_2 \in SE(3)$ because we require all input PCs, *i.e.*, X_i, $g_i X_i$, $i = 1, 2$, to be centered.

Then we recall Def. 3.1 for pair-wise assembly tasks:

Definition B.2 (Restate $SO(3)^2$-equivariance and $SO(3)$-invariance in Def. 3.1 for pair-wise problems)**.** Let X_1, X_2 be the input PCs and $P \in \mu(SE(3) \times SE(3))$.

- P is $SO(3)^2$-equivariant if $P(A|X_1, X_2) = P(A(g_1^{-1}, g_2^{-1})|g_1 X_1, g_2 X_2)$ for all $g_1, g_2 \in SO(3)$ and $A \subseteq SO(3) \times SO(3)$, where $A(g_1^{-1}, g_2^{-1}) = \{(a_1 g_1^{-1}, a_2 g_2^{-1}) : (a_1, a_2) \in A\}$.
- P is $SO(3)$-invariance if $P(A|X_1, X_2) = P(rA|X_1, X_2)$ for all $r \in SO(3)$ and $A \subseteq SO(3) \times SO(3)$.

Intuitively, both Def. B.1 and Def. B.2 describe the equivariance property of an assembly solution, and the only difference is that Def. B.1 describes the special case where X_1 can be rigidly transformed and X_2 is fixed, while Def. B.2 describes the solution where both X_1 and X_2 can be rigidly transformed. In other words, a solution satisfying Def. B.2 can be converted to a solution satisfying Def. B.1 by fixing X_2. Formally, we have the following proposition.

Proposition B.3. *Let P be $SO(3)^2$-equivariant and $SO(3)$-invariant. If $\tilde{P}(A|X_1, X_2) \triangleq P(A \times \{e\}|X_1, X_2)$ for $A \subseteq SO(3)$, then $\tilde{P}$ is bi-equivariant.*

Proof. We prove this proposition by directly verifying the definition.

$$\begin{aligned}
\tilde{P}(g_2 A g_1^{-1}|g_1 X_1, g_2 X_2) &= P(g_2 A g_1^{-1} \times \{e\}|g_1 X_1, g_2 X_2) &(16)\\
&= P(g_2 A \times \{e\}|X_1, g_2 X_2) &(17)\\
&= P(A \times \{g_2^{-1}\}|X_1, g_2 X_2) &(18)\\
&= P(A \times \{e\}|X_1, X_2) &(19)\\
&= \tilde{P}(A|X_1, X_2). &(20)
\end{aligned}$$

Here, the second and the fourth equation hold because P is $SO(3)^2$-equivariant, the third equation holds because P is $SO(3)$-invariant, and the first and last equation are due to the definition. □

We note that the deterministic definition of bi-equivariance in [40] is a special case of Def. B.1, where $\hat{P}$ is a Dirac delta function. In addition, as discussed in Appx. E in [40], a major limitation of the deterministic definition of bi-equivariance is that it cannot handle symmetric shapes. In contrast, it is straightforward to see that the probabilistic definition, *i.e.*, both Def. B.1 and Def. B.2 are free from this issue. Here, we consider the example in [40]. Assume that X_1 is symmetric, *i.e.*, there exists $g_1 \in SO(3)$ such that $g_1 X_1 = X_1$. Under Def. B.1, we have $P(A|X_1, X_2) = P(A|g_1 X_1, X_2) = P(A g_1|X_1, X_2)$, which simply means that $P(A|X_1, X_2)$ is $\mathcal{R}_{g_1}$-invariant. Note that this will not cause any contradiction, *i.e.*, the feasible set is not empty. For example, a uniform distribution on $SO(3)$ is $\mathcal{R}_{g_1}$-invariant.

As for the permutation-equivariance, the swap-equivariance in [40] is a deterministic pair-wise version of the permutation-equivariance in Def. B.2, and they both mean that the assembled shape is independent of the order of the input pieces.

C Proofs

C.1 Proof in Sec. 4.2

To prove Thm. 4.2, which established the relations between related vector fields and equivariant distributions, we proceed in two steps: first, we prove lemma C.1, which connects related vector fields to equivariant mappings; then we prove lemma. C.2, which connects equivariant mappings to equivariant distributions.

Lemma C.1. *Let G be a smooth manifold, $F : G \to G$ be a diffeomorphism. If vector field v_τ is F-related to vector field w_τ for $\tau \in [0, 1]$, then $F \circ \phi_\tau = \psi_\tau \circ F$, where ϕ_τ and ψ_τ are generated by v_τ and w_τ respectively.*

Proof. Let $\tilde{\psi}_\tau \triangleq F \circ \phi_\tau \circ F^{-1}$. We only need to show that $\tilde{\psi}_\tau$ coincides with ψ_τ.

We consider a curve $\tilde{\psi}_\tau(F(\boldsymbol{g}_0))$, $\tau \in [0, 1]$, for a arbitrary $\boldsymbol{g}_0 \in G$. We first verify that $\tilde{\psi}_0(F(\boldsymbol{g}_0)) = F \circ \phi_0 \circ F^{-1} \circ F(\boldsymbol{g}_0) = F(\boldsymbol{g}_0)$. Note that the second equation holds because $\phi_0(\boldsymbol{g}_0) = \boldsymbol{g}_0$, *i.e.*, ϕ_τ

is an integral path. Then we verify

$$\begin{aligned}
\frac{\partial}{\partial\tau}(\tilde{\psi}_\tau(F(\boldsymbol{g}_0))) =& \frac{\partial}{\partial\tau}(F\circ\phi_\tau(\boldsymbol{g}_0)) && (21)\\
=& F_{*,\phi_\tau(\boldsymbol{g}_0)}\circ\frac{\partial}{\partial\tau}(\phi_\tau(\boldsymbol{g}_0)) && (22)\\
=& F_{*,\phi_\tau(\boldsymbol{g}_0)}\circ v_\tau(\phi_\tau(\boldsymbol{g}_0)) && (23)\\
=& w_\tau(F\circ\phi_\tau(\boldsymbol{g}_0)) && (24)\\
=& w_\tau(\tilde{\psi}_\tau(F(\boldsymbol{g}_0))) && (25)
\end{aligned}$$

where the 2-nd equation holds due to the chain rule, and the 4-th equation holds becomes v_τ is F-related to w_τ. Therefore, we can conclude that $\tilde{\psi}_\tau(F(\boldsymbol{g}_0))$ is an integral curve generated by w_τ starting from $F(\boldsymbol{g}_0)$. However, by definition of ψ_τ, $\psi_\tau(F(\boldsymbol{g}_0))$ is also the integral curve generated by w_τ and starts from $F(\boldsymbol{g}_0)$. Due to the uniqueness of integral curves, we have $\tilde{\psi}_\tau = \psi_\tau$. □

Lemma C.2. *Let ϕ, ψ, $F: G\to G$ be three diffeomorphisms satisfying $F\circ\phi = \psi\circ F$. We have $F_\#(\phi_\#\rho) = \psi_\#(F_\#\rho)$ for all distribution ρ on G.*

Proof. Let $A\subseteq G$ be a measurable set. We first verify that $\phi^{-1}(F^{-1}(A)) = F^{-1}(\psi^{-1}(A))$: If $x\in\phi^{-1}(F^{-1}(A))$, then $(F\circ\phi)(x)\in A$. Since $F\circ\phi = \psi\circ F$, we have $(\psi\circ F)(x)\in A$, which implies $x\in F^{-1}(\psi^{-1}(A))$, *i.e.*, $\phi^{-1}(F^{-1}(A))\subseteq F^{-1}(\psi^{-1}(A))$. The other side can be verified similarly. Then we have

$$(F_\#(\phi_\#\rho))(A) = \rho(\phi^{-1}(F^{-1}(A))) = \rho(F^{-1}(\psi^{-1}(A))) = (\psi_\#(F_\#\rho))(A), \tag{26}$$

which proves the lemma. □

Now, we can prove Thm. 4.2 using the above two lemmas.

Proof of Thm. 4.2. Since v_X is F-related to v_Y, according to lemma C.1, we have $F\circ\phi_X = \phi_Y\circ F$. Then according to lemma C.2, we have $F_\#(\phi_{X\#}P_0) = \phi_{Y\#}(F_\#P_0)$. The proof is complete by letting $P_X = \phi_{X\#}P_0$ and $P_Y = \phi_{Y\#}(F_\#P_0)$. □

We remark that our theory extends the results in [20], where only invariance is considered, Specifically, we have the following corollary.

Corollary C.3 (Thm 2 in [20])**.** *Let G be the Euclidean space, F be a diffeomorphism on G, and v_τ be a F-invariant vector field,* i.e.*, v_τ is F-related to v_τ, then we have $F\circ\phi_\tau = \phi_\tau\circ F$, where ϕ_τ is generated by v_τ.*

Proof. This is a direct consequence of lemma. C.1 where G is the Euclidean space and $w_\tau = v_\tau$. □

Note that the terminology used in [20] is different from ours: The F-invariant vector fields in our work is called F-equivariant vector field in [20], and [20] does not consider general related vector fields.

Finally, we present the proof of Prop. 4.5 and Prop. 4.6.

Proof of Prop. 4.5. If v_X is $\mathcal{R}_{\boldsymbol{g}^{-1}}$-related to $v_{\boldsymbol{g}X}$, we have $v_{\boldsymbol{g}X}(\hat{\boldsymbol{g}}\boldsymbol{g}^{-1}) = (\mathcal{R}_{\boldsymbol{g}^{-1}})_{*,\hat{\boldsymbol{g}}}v_X(\hat{\boldsymbol{g}})$ for all $\hat{\boldsymbol{g}},\boldsymbol{g}\in SE(3)^N$. By letting $\boldsymbol{g}=\hat{\boldsymbol{g}}$, we have

$$v_X(\boldsymbol{g}) = (\mathcal{R}_{\boldsymbol{g}})_{*,e}v_{\boldsymbol{g}X}(e) \tag{27}$$

where $(\mathcal{R}_{\boldsymbol{g}})_{*,e} = \left((\mathcal{R}_{\boldsymbol{g}^{-1}})_{*,\boldsymbol{g}}\right)^{-1}$ due to the chain rule of $\mathcal{R}_{\boldsymbol{g}}\mathcal{R}_{\boldsymbol{g}^{-1}} = e$.

On the other hand, if Eqn. (27) holds, we have

$$(\mathcal{R}_{\boldsymbol{g}^{-1}})_{*,\hat{\boldsymbol{g}}}v_X(\hat{\boldsymbol{g}}) = (\mathcal{R}_{\boldsymbol{g}^{-1}})_{*,\hat{\boldsymbol{g}}}(\mathcal{R}_{\hat{\boldsymbol{g}}})_{*,e}v_{\hat{\boldsymbol{g}}X}(e) = (\mathcal{R}_{\hat{\boldsymbol{g}}\boldsymbol{g}^{-1}})_{*,e}v_{\hat{\boldsymbol{g}}X}(e) = v_{\boldsymbol{g}X}(\hat{\boldsymbol{g}}\boldsymbol{g}^{-1}), \tag{28}$$

which suggests that v_X is $\mathcal{R}_{\boldsymbol{g}^{-1}}$-related to $v_{\boldsymbol{g}X}$. Note that the second equation holds due to the chain rule of $\mathcal{R}_{\boldsymbol{g}^{-1}}\mathcal{R}_{\hat{\boldsymbol{g}}} = \mathcal{R}_{\hat{\boldsymbol{g}}\boldsymbol{g}^{-1}}$, and the first and the third equation are the result of Eqn. (27). □

Proof of Prop. 4.6. 1) Assume v_X is σ-related to $v_{\sigma X}$: $(\sigma)_{*,g} v_X(g) = V_{\sigma X}(\sigma(g))$. By inserting Eqn. (5) to this equation, we have

$$(\sigma)_{*,\boldsymbol{g}}(\mathcal{R}_{\boldsymbol{g}})_{*,e} f(\boldsymbol{g}X) = (\mathcal{R}_{\sigma \boldsymbol{g}})_{*,e} f(\sigma(\boldsymbol{g})\sigma(X)). \tag{29}$$

Since $\sigma \circ \mathcal{R}_{\boldsymbol{g}} = \mathcal{R}_{\sigma \boldsymbol{g}} \circ \sigma$, by the chain rule, we have $\sigma_*(\mathcal{R}_{\boldsymbol{g}})_* = (\mathcal{R}_{\sigma \boldsymbol{g}})_* \sigma_*$. In addition, $\sigma(\boldsymbol{g})\sigma(X) = \sigma(\boldsymbol{g}X)$. Thus, this equation can be simplified as

$$(\mathcal{R}_{\sigma \boldsymbol{g}})_* \sigma_* f(\boldsymbol{g}X) = (\mathcal{R}_{\sigma \boldsymbol{g}})_{*,e} f(\sigma(\boldsymbol{g}X)) \tag{30}$$

which suggests

$$\sigma_* f = f \circ \sigma. \tag{31}$$

The first statement in Prop. 4.6 can be proved by reversing the discussion.

2) Assume v_X is $\mathcal{L}_r$-related to v_X: $(\mathcal{L}_r)_{*,g} v_X(\boldsymbol{g}) = V_X(r\boldsymbol{g})$. By inserting Eqn. (5) to this equation, we have

$$(\mathcal{L}_r)_{*,g}(\mathcal{R}_{\boldsymbol{g}})_{*,e} f(\boldsymbol{g}X) = (\mathcal{R}_{r\boldsymbol{g}})_{*,e} f(r\boldsymbol{g}X). \tag{32}$$

Since $\mathcal{R}_{r\boldsymbol{g}} = \mathcal{R}_{\boldsymbol{g}} \circ \mathcal{R}_r$, by the chain rule, we have $(\mathcal{R}_{r\boldsymbol{g}})_{*,e} = (\mathcal{R}_{\boldsymbol{g}})_{*,r}(\mathcal{R}_r)_{*,e}$. In addition, $(\mathcal{L}_r)(\mathcal{R}_{\boldsymbol{g}}) = (\mathcal{R}_g)(\mathcal{L}_r)$, by the chain rule, we have $(\mathcal{L}_r)_{*,\boldsymbol{g}}(\mathcal{R}_{\boldsymbol{g}})_{*,e} = (\mathcal{R}_{\boldsymbol{g}})_{*,r}(\mathcal{L}_r)_{*,e}$. Thus the above equation can be simplified as

$$(\mathcal{L}_r)_{*,e} f(\boldsymbol{g}X) = (\mathcal{R}_r)_{*,e} f(r\boldsymbol{g}X) \tag{33}$$

which implies

$$f \circ r = (\mathcal{R}_{r^{-1}})_{*,r} \circ (\mathcal{L}_r)_{*,e} \circ f. \tag{34}$$

By representing f in the matrix form, we have

$$w^i_\times(rX) = r w^i_\times(X) r^T \tag{35}$$

$$t^i(rX) = r t^i(X) \tag{36}$$

for all i, where r on the right hand side represents the matrix form of the rotation r. Here the first equation can be equivalently written as $w^i(rX) = r w^i(X)$. The second statement in Prop. 4.6 can be proved by reversing the discussion. □

C.2 Proofs in Sec. 4.3

To establish the results in this section, we need to assume the uniqueness of r^* (6):

Assumption C.4. The solution to (6) is unique.

Note that this assumption is mild. A sufficient condition [40] of assumption C.4 is that the singular values of $\tilde{\boldsymbol{g}}_1^T \boldsymbol{g}_0 \in \mathbb{R}^{3\times 3}$ satisfy $\sigma_1 \geq \sigma_2 > \sigma_3 \geq 0$, *i.e.*, σ_2 and σ_3 are not equal. We leave the more general treatment without requiring the uniqueness of r^* to future work.

We first justify the definition of $\boldsymbol{g}_1 = r^* \tilde{\boldsymbol{g}}_1$ by showing that $\boldsymbol{g}_1$ follows P_1 in the following proposition.

Proposition C.5. *Let P_0 and P_1 be two $SO(3)$-invariant distributions, and $\boldsymbol{g}_0$, $\tilde{\boldsymbol{g}}_1$ be independent samples from P_0 and P_1 respectively. If r^* is given by (6) and assumption C.4 holds, then $\boldsymbol{g}_1 = r^* \tilde{\boldsymbol{g}}_1$ follows P_1.*

Proof. Define $A_{\tilde{\boldsymbol{g}}_1} = \{\boldsymbol{g}_0 | r^*(\boldsymbol{g}_0, \tilde{\boldsymbol{g}}_1) = e\}$, where we write r^* as a function of $\tilde{\boldsymbol{g}}_1$ and $\boldsymbol{g}_0$. Then we have $P(r^* = e|\tilde{\boldsymbol{g}}_1) = P_0(A_{\tilde{\boldsymbol{g}}_1})$ by definition. In addition, due to the uniqueness of the solution to (6), for an arbitrary $\hat{r} \in SO(3)$, we have $P(r^* = \hat{r}|\tilde{\boldsymbol{g}}_1) = P_0(\hat{r}A_{\tilde{\boldsymbol{g}}_1})$. Since P_0 is $SO(3)$-invariant, we have $P_0(\hat{r}A_{\tilde{\boldsymbol{g}}_1}) = P_0(A_{\tilde{\boldsymbol{g}}_1})$, thus, $P(r^* = \hat{r}|\tilde{\boldsymbol{g}}_1) = P(r^* = e|\tilde{\boldsymbol{g}}_1)$. In other words, for a given $\tilde{\boldsymbol{g}}_1$, r^* follows the uniform distribution $U_{SO(3)}$.

Finally we compute the probability density of $\boldsymbol{g}_1$:

$$P(\boldsymbol{g}_1) = \int P(r^* = \hat{r}^{-1} | \hat{r}\boldsymbol{g}_1) P_1(\hat{r}\boldsymbol{g}_1) d\hat{r} \tag{37}$$

$$= \int U_{SO(3)}(\hat{r}) P_1(\boldsymbol{g}_1) d\hat{r} \tag{38}$$

$$= P_1(\boldsymbol{g}_1), \tag{39}$$

which suggests that $\boldsymbol{g}_1$ follows P_1. Here the second equation holds because P_1 is $SO(3)$-invariant. □

Then we discuss the equivariance of the constructed h_X (7).

Proposition C.6. *Given* $\boldsymbol{r} \in SO(3)^N$, $\boldsymbol{g}_0, \tilde{\boldsymbol{g}}_1 \in SE(3)^N$, $\sigma \in S_N$, $r \in SO(3)$ *and* $\tau \in [0,1]$. *Let* h_X *be a path generated by* $\boldsymbol{g}_0$ *and* $\tilde{\boldsymbol{g}}_1$. *Under assumption C.4,*

- *if* $h_{\boldsymbol{r}X}$ *is generated by* $\boldsymbol{g}_0\boldsymbol{r}^{-1}$ *and* $\tilde{\boldsymbol{g}}_1\boldsymbol{r}^{-1}$, *then* $h_{\boldsymbol{r}X}(\tau) = \mathcal{R}_{\boldsymbol{r}^{-1}} h_X(\tau)$.
- *if* $h_{\sigma X}$ *is generated by* $\sigma(\boldsymbol{g}_0)$ *and* $\sigma(\tilde{\boldsymbol{g}}_1)$, *then* $h_{\sigma X}(\tau) = \sigma(h_X(\tau))$.
- *if* $\hat{h}_X$ *is generated by* $r\boldsymbol{g}_0$ *and* $r\tilde{\boldsymbol{g}}_1$, *then* $\hat{h}_X(\tau) = \mathcal{L}_r(h_X(\tau))$.

Proof. 1) Due to the uniqueness of the solution to (6), we have $r^*(\boldsymbol{g}_0\boldsymbol{r}^{-1}, \tilde{\boldsymbol{g}}_1\boldsymbol{r}^{-1}) = r^*(\boldsymbol{g}_0, \tilde{\boldsymbol{g}}_1)$. Thus, we have

$$h_{\boldsymbol{r}X}(\tau) = \exp(\tau \log(\boldsymbol{g}_1\boldsymbol{g}_0^{-1}))\boldsymbol{g}_0\boldsymbol{r}^{-1} = \mathcal{R}_{\boldsymbol{r}^{-1}}(h_{\boldsymbol{r}X}(\tau)). \tag{40}$$

2) Due to the uniqueness of the solution to (6), we have $r^*(\sigma(\boldsymbol{g}_0), \sigma(\tilde{\boldsymbol{g}}_1)) = \sigma(r^*(\boldsymbol{g}_0, \tilde{\boldsymbol{g}}_1))$. Thus, we have $\sigma(h_X) = h_{\sigma X}$.

3) Due to the uniqueness of the solution to (6), we have $r^*(r\boldsymbol{g}_0, r\tilde{\boldsymbol{g}}_1) = rr^*(\boldsymbol{g}_0, \tilde{\boldsymbol{g}}_1)r^{-1}$. Thus,

$$\hat{h}_{rX}(\tau) = \exp(\tau \log(rr^*\tilde{\boldsymbol{g}}_1\boldsymbol{g}_0^{-1}r^{-1}))r\boldsymbol{g}_0 = r\exp(\tau\log(r^*\tilde{\boldsymbol{g}}_1\boldsymbol{g}_0^{-1}))\boldsymbol{g}_0 = \mathcal{L}_r(h_X(\tau)). \tag{41}$$

□

With the above preparation, we can finally prove Prop. 4.7.

Proof of Prop. 4.7. 1) By definition

$$L(\boldsymbol{r}X) = \mathbb{E}_{\tau, \boldsymbol{g}_0' \sim P_0, \tilde{\boldsymbol{g}}_1' \sim P_{\boldsymbol{r}X}} ||v_{\boldsymbol{r}X}(h_{\boldsymbol{r}X}(\tau)) - \frac{\partial}{\partial \tau} h_{\boldsymbol{r}X}(\tau)||_F^2, \tag{42}$$

where $h_{\boldsymbol{r}X}$ is the path generated by $\boldsymbol{g}_0'$ and $\tilde{\boldsymbol{g}}_1'$. Since $P_0 = (\mathcal{R}_{\boldsymbol{r}^{-1}})_\# P_0$ and $P_{\boldsymbol{r}X} = (\mathcal{R}_{\boldsymbol{r}^{-1}})_\# P_X$ by assumption, we can write $\boldsymbol{g}_0' = \boldsymbol{g}_0\boldsymbol{r}^{-1}$ and $\tilde{\boldsymbol{g}}_1' = \tilde{\boldsymbol{g}}_1\boldsymbol{r}^{-1}$, where $\boldsymbol{g}_0 \sim P_0$ and $\tilde{\boldsymbol{g}}_1 \sim P_X$. According to the first part of Prop. C.6, we have $h_{\boldsymbol{r}X}(\tau) = \mathcal{R}_{\boldsymbol{r}^{-1}} h_X(\tau)$, where h_X is a path generated by $\boldsymbol{g}_0$ and $\tilde{\boldsymbol{g}}_1$. By taking derivative on both sides of the equation, we have $\frac{\partial}{\partial\tau} h_{\boldsymbol{r}X}(\tau) = (\mathcal{R}_{\boldsymbol{r}^{-1}})_{*, h_X(\tau)} \frac{\partial}{\partial\tau} h_X(\tau)$. Then we have

$$L(\boldsymbol{r}X) = \mathbb{E}_{\tau, \boldsymbol{g}_0' \sim P_0, \tilde{\boldsymbol{g}}_1' \sim P_{\boldsymbol{r}X}} ||v_{\boldsymbol{r}X}(\mathcal{R}_{\boldsymbol{r}^{-1}} h_X(\tau)) - (\mathcal{R}_{\boldsymbol{r}^{-1}})_{*, h_X(\tau)} \frac{\partial}{\partial \tau} h_X(\tau)||_F^2 \tag{43}$$

by inserting these two equations into Eqn. (42). Since v_X is $\mathcal{R}_{\boldsymbol{r}^{-1}}$-related to $v_{\boldsymbol{r}X}$ by assumption, we have $v_{\boldsymbol{r}X}(\mathcal{R}_{\boldsymbol{r}^{-1}} h_X(\tau)) = (\mathcal{R}_{\boldsymbol{r}^{-1}})_{*, h_X(\tau)} v_X(h_X(\tau))$. Thus, we have

$$\begin{aligned} ||v_{\boldsymbol{r}X}(\mathcal{R}_{\boldsymbol{r}^{-1}} h_X(\tau)) - (\mathcal{R}_{\boldsymbol{r}^{-1}})_{*, h_X(\tau)} \frac{\partial}{\partial \tau} h_X(\tau)||_F^2 &= ||(\mathcal{R}_{\boldsymbol{r}^{-1}})_{*, h_X(\tau)} (v_{\boldsymbol{r}X}(h_X(\tau)) - \frac{\partial}{\partial \tau} h_X(\tau))||_F^2 \\ &= ||(v_{\boldsymbol{r}X}(h_X(\tau)) - \frac{\partial}{\partial \tau} h_X(\tau))||_F^2 \end{aligned} \tag{44}$$

where the second equation holds because $(\mathcal{R}_{\boldsymbol{r}^{-1}})_{*, h_X(\tau)}$ is an orthogonal matrix. The desired result follows.

2) The second statement can be proved similarly as the first one, where σ-equivariance is considered instead of $\mathcal{R}_{\boldsymbol{r}^{-1}}$-equivariance.

3) Denote $\boldsymbol{g}_0' = r\boldsymbol{g}_0$ and $\tilde{\boldsymbol{g}}_1' = r\tilde{\boldsymbol{g}}_1$, where $\boldsymbol{g}_0 \sim P_0$ and $\tilde{\boldsymbol{g}}_1 \sim P_X$. According to the third part of Prop. C.6, we have $\hat{h}_X(\tau) = \mathcal{L}_r(h_X(\tau))$. By taking derivative on both sides of the equation, we have $\frac{\partial}{\partial\tau}\hat{h}_X(\tau) = (\mathcal{L}_r)_{*, h_X(\tau)} \frac{\partial}{\partial\tau} h_X(\tau)$. Then the rest of the proof can be conducted similarly to the first part of the proof. □

D $SO(2)$-reduction

The main idea of $SO(2)$-reduction [] is to rotate the edge uv to the y-axis, and then update node feature in the rotated space. Since all 3D rotations are reduced to 2D rotations about the y-axis in the rotated space, the feature update rule is greatly simplified.

Here, we describe this technique in the matrix form to facilitates better parallelization. The original element form description can be found in []. Let $F_v^l \in \mathbb{R}^{c\times(2l+1)}$ be a c-channel l-degree feature of point v, and $L > 0$ be the maximum degree of features. We construct $\hat{F}_v^l \in \mathbb{R}^{c\times(2L+1)}$ by padding F_v^l with $L - l$ zeros at the beginning and the end of the feature, then we define the full feature $F_v \in \mathbb{R}^{c\times L\times(2L+1)}$ as the concatenate of all $\hat{F}_v^l$ with $0 < l \leq L$. For an edge vu, there exists a rotation r_{vu} that aligns uv to the y-axis. We define $R_{vu} \in \mathbb{R}^{L\times(2L+1)\times(2L+1)}$ to be the full rotation matrix, where the l-th slice $R_{vu}[l, :, :]$ is the l-th Wigner-D matrix of r_{vu} with zeros padded at the boundary. K_v defined in (11) can be efficiently computed as

$$K_v = R_{vu}^T \times_{1,2} (W_K \times_3 (D_K \times_{1,2} R_{vu} \times_{1,2} F_v)), \tag{45}$$

where $M_1 \times_i M_2$ represents the batch-wise multiplication of M_1 and M_2 with the i-th dimension of M_2 treated as the batch dimension. $W_K \in \mathbb{R}^{(cL)\times(cL)}$ is a learnable weight, $D_K \in \mathbb{R}^{c\times(2L+1)\times(2L+1)}$ is a learnable matrix taking the form of 2D rotations about the y-axis, *i.e.*, for each i, $D_K[i, :, :]$ is

$$\begin{bmatrix}
a_1 & & & & & & & & -b_1 \\
 & a_2 & & & & & & -b_2 & \\
 & & \ddots & & & & \iddots & & \\
 & & & a_{L-1} & & -b_{L-1} & & & \\
 & & & & a_L & & & & \\
 & & & b_{L-1} & & a_{L-1} & & & \\
 & & \iddots & & & & \ddots & & \\
 & b_2 & & & & & & a_2 & \\
b_1 & & & & & & & & a_1
\end{bmatrix}, \tag{46}$$

where $a_1, \cdots, a_L, b_1, \cdots, b_{L-1} : \mathbb{R}_+ \to \mathbb{R}$ are learnable functions that map $|vu|$ to the coefficients. V_v defined in (11) can be computed similarly. Note that (45) does not require the computation of Clebsch-Gordan coefficients, the spherical harmonic functions, and all computations are in the matrix form where no for-loop is needed, so it is much faster than the computations in (11).

E More details of Sec. 6

We present more details of Eda on 3DL in Fig. 5. We observe that the vector field is is gradually learned during training, *i.e.*, the training error converges. On the test set, RK4 outperforms the RK1, and they both benefit from more time steps, especially for rotation errors.

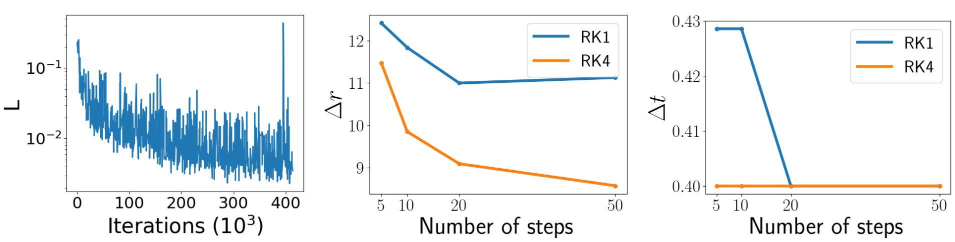

Figure 5: More details of Eda on 3DL. Left: the training curve. Middle and right: the influence of RK4/RK1 and the number of time steps on Δr and Δt.

We provide the complete version of Table 2 in Table 5, where we additionally report the standard deviations of Eda.

We provide some qualitative results on BB datasets in Fig. 6 and Fig. 8. Eda can generally recover the shape of the objects except for some rare cases, such as the $3rd$ sample in the second row in Fig. 6. We hypothesize that Eda can achieve better performance when using finer grained inputs. A complete version of Tab. 3 is provided in Tab. 6, where we additionally report the standard deviations of Eda.

We provide a few examples of the reconstructed road views in Fig. 9.

Table 5: The complete version of Table 2 with stds of Eda reported in bracked.

	3DM		3DL		3DZ	
	Δr	Δt	Δr	Δt	Δr	Δt
FGR	69.5	0.6	117.3	1.3	–	–
GEO	7.43	0.19	28.38	0.69	–	–
ROI (500)	5.64	0.15	21.94	0.53	–	–
ROI (5000)	5.44	0.15	22.17	0.53	–	–
AMR	5.0	**0.13**	20.5	0.53	–	–
Eda (RK4, 50)	**2.38** (0.16)	0.16 (0.01)	**8.57** (0.08)	**0.4** (0.0)	78.74 (0.6)	0.96 (0.01)

Table 6: The complete version of Table 3 with stds of Eda reported in brackets.

	Δr	Δt	Time (min)
GLO	126.3	0.3	0.9
DGL	125.8	0.3	0.9
LEV	125.9	0.3	8.1
Eda (RK1, 10)	80.64	0.16	19.4
Eda (RK4, 10)	79.2 (0.58)	0.16 (0.0)	76.9

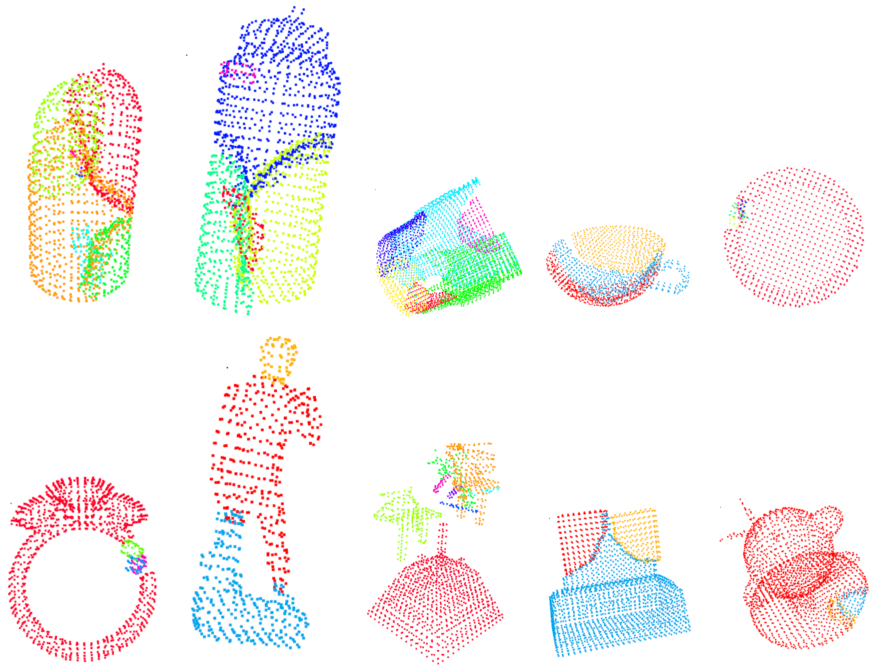

(a) Random samples of Eda

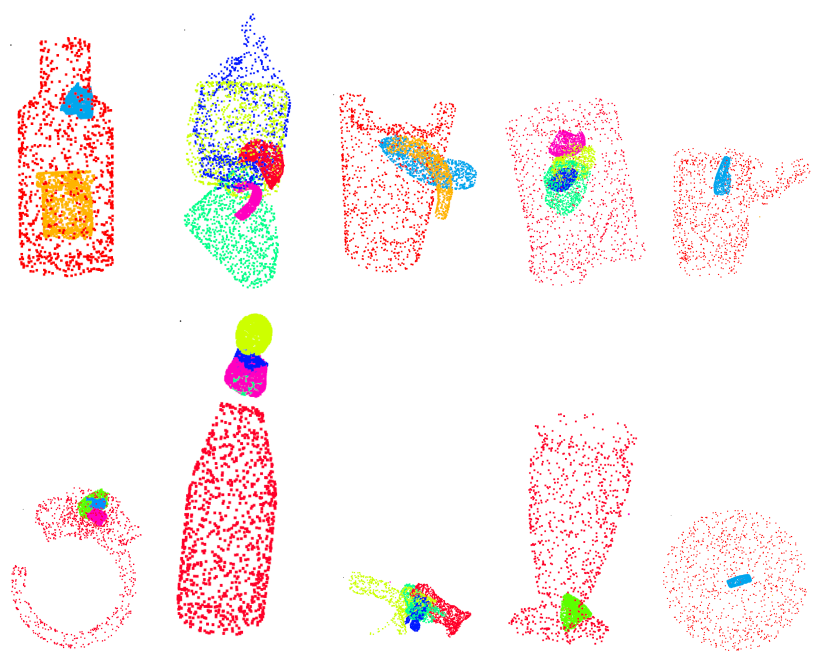

(b) Random samples of DGL

Figure 6: Qualitative results of Eda and DGL.

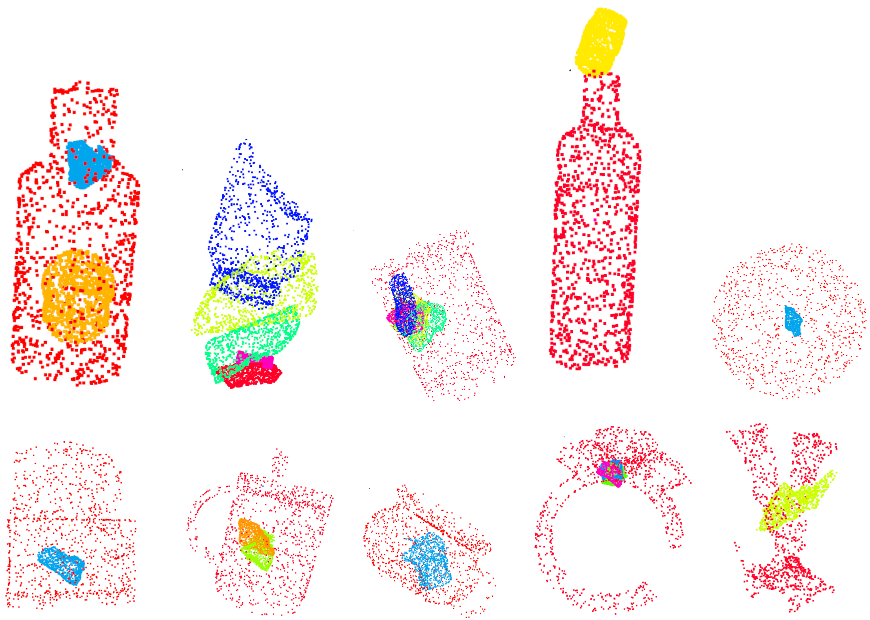

(a) Random samples of GLO

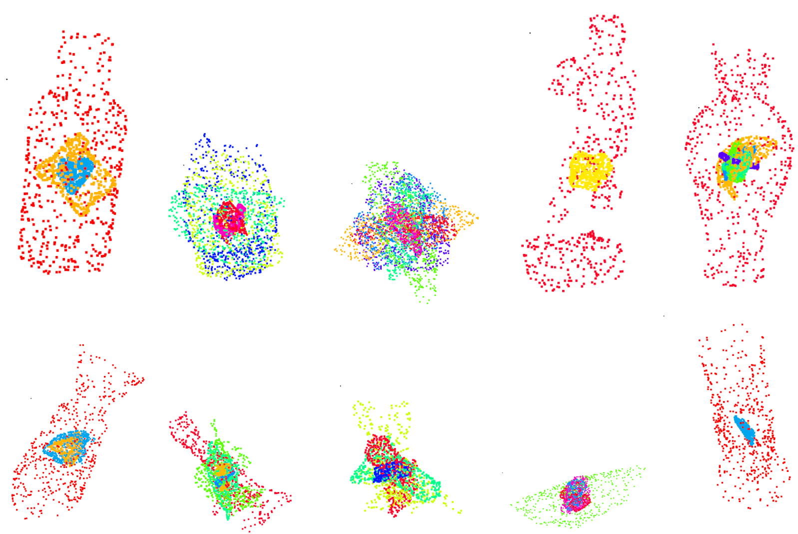

(b) Random samples of LEV

Figure 7: Qualitative results of GLO and LEV.

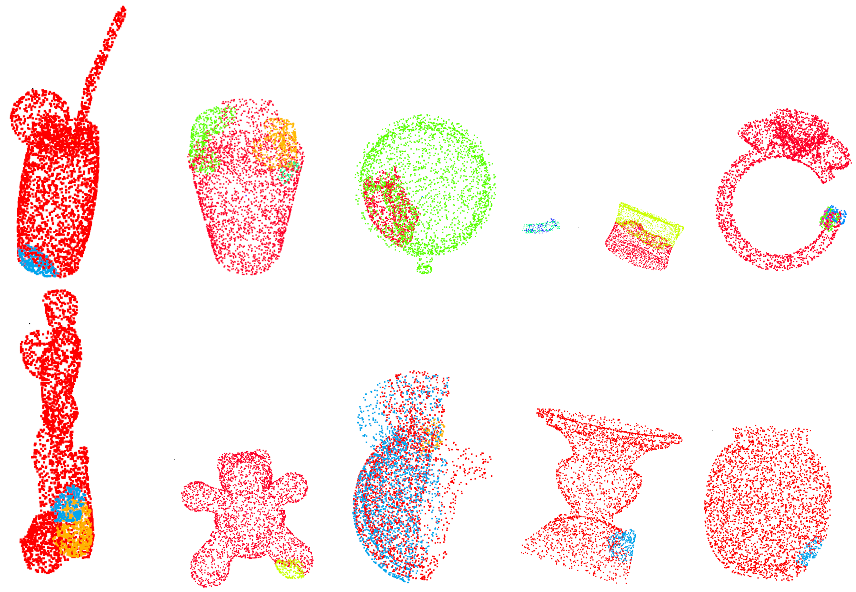

(a) Random samples of JIG

Figure 8: Qualitative results of JIG.

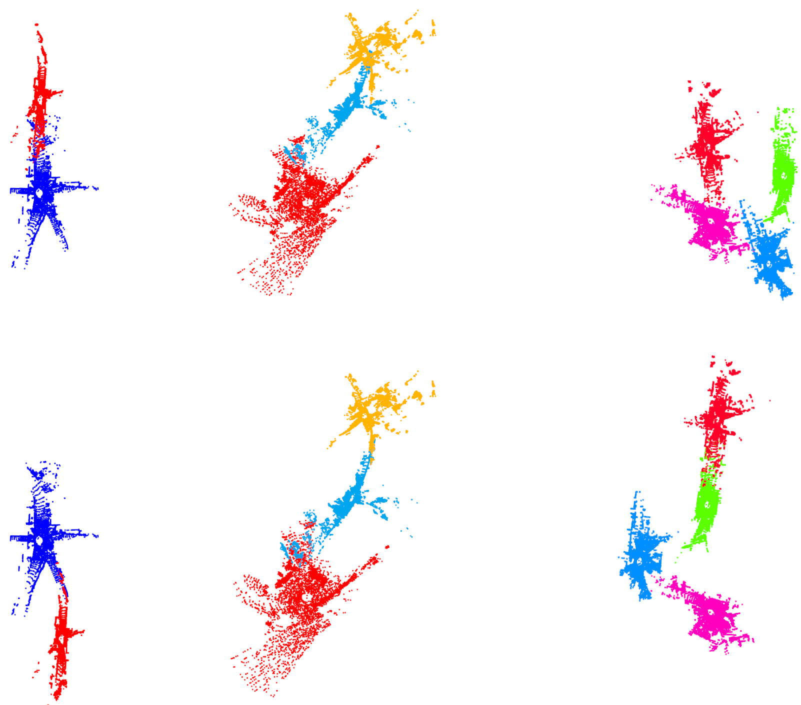

(a) 2-piece assembly (b) 3-piece assembly (c) 4-piece assembly

Figure 9: Qualitative results of Eda on kitti. We present the results of Eda (1-st row) and the ground truth (2-nd row). For each assembly, Eda correctly places the input road views on the same plane.

NeurIPS Paper Checklist

1. **Claims**

   Question: Do the main claims made in the abstract and introduction accurately reflect the paper's contributions and scope?

   Answer: [Yes]

   Justification: We claim a new equivariant flow matching method, called Eda, for multi-piece assembly tasks in the abstract and introduction. This is the main contribution of the paper.

   Guidelines:

   - The answer NA means that the abstract and introduction do not include the claims made in the paper.
   - The abstract and/or introduction should clearly state the claims made, including the contributions made in the paper and important assumptions and limitations. A No or NA answer to this question will not be perceived well by the reviewers.
   - The claims made should match theoretical and experimental results, and reflect how much the results can be expected to generalize to other settings.
   - It is fine to include aspirational goals as motivation as long as it is clear that these goals are not attained by the paper.

2. **Limitations**

   Question: Does the paper discuss the limitations of the work performed by the authors?

   Answer: [Yes]

   Justification: We discuss the limitations/future research directions in Sec. 7.

   Guidelines:

   - The answer NA means that the paper has no limitation while the answer No means that the paper has limitations, but those are not discussed in the paper.
   - The authors are encouraged to create a separate "Limitations" section in their paper.
   - The paper should point out any strong assumptions and how robust the results are to violations of these assumptions (e.g., independence assumptions, noiseless settings, model well-specification, asymptotic approximations only holding locally). The authors should reflect on how these assumptions might be violated in practice and what the implications would be.
   - The authors should reflect on the scope of the claims made, e.g., if the approach was only tested on a few datasets or with a few runs. In general, empirical results often depend on implicit assumptions, which should be articulated.
   - The authors should reflect on the factors that influence the performance of the approach. For example, a facial recognition algorithm may perform poorly when image resolution is low or images are taken in low lighting. Or a speech-to-text system might not be used reliably to provide closed captions for online lectures because it fails to handle technical jargon.
   - The authors should discuss the computational efficiency of the proposed algorithms and how they scale with dataset size.
   - If applicable, the authors should discuss possible limitations of their approach to address problems of privacy and fairness.
   - While the authors might fear that complete honesty about limitations might be used by reviewers as grounds for rejection, a worse outcome might be that reviewers discover limitations that aren't acknowledged in the paper. The authors should use their best judgment and recognize that individual actions in favor of transparency play an important role in developing norms that preserve the integrity of the community. Reviewers will be specifically instructed to not penalize honesty concerning limitations.

3. **Theory assumptions and proofs**

   Question: For each theoretical result, does the paper provide the full set of assumptions and a complete (and correct) proof?

   Answer: [Yes]

Justification: All proofs can be found in Sec. C

Guidelines:

- The answer NA means that the paper does not include theoretical results.
- All the theorems, formulas, and proofs in the paper should be numbered and cross-referenced.
- All assumptions should be clearly stated or referenced in the statement of any theorems.
- The proofs can either appear in the main paper or the supplemental material, but if they appear in the supplemental material, the authors are encouraged to provide a short proof sketch to provide intuition.
- Inversely, any informal proof provided in the core of the paper should be complemented by formal proofs provided in appendix or supplemental material.
- Theorems and Lemmas that the proof relies upon should be properly referenced.

4. **Experimental result reproducibility**

   Question: Does the paper fully disclose all the information needed to reproduce the main experimental results of the paper to the extent that it affects the main claims and/or conclusions of the paper (regardless of whether the code and data are provided or not)?

   Answer: [Yes]

   Justification: The details of the experiments are provided in Sec. 6.1,

   Guidelines:

   - The answer NA means that the paper does not include experiments.
   - If the paper includes experiments, a No answer to this question will not be perceived well by the reviewers: Making the paper reproducible is important, regardless of whether the code and data are provided or not.
   - If the contribution is a dataset and/or model, the authors should describe the steps taken to make their results reproducible or verifiable.
   - Depending on the contribution, reproducibility can be accomplished in various ways. For example, if the contribution is a novel architecture, describing the architecture fully might suffice, or if the contribution is a specific model and empirical evaluation, it may be necessary to either make it possible for others to replicate the model with the same dataset, or provide access to the model. In general. releasing code and data is often one good way to accomplish this, but reproducibility can also be provided via detailed instructions for how to replicate the results, access to a hosted model (e.g., in the case of a large language model), releasing of a model checkpoint, or other means that are appropriate to the research performed.
   - While NeurIPS does not require releasing code, the conference does require all submissions to provide some reasonable avenue for reproducibility, which may depend on the nature of the contribution. For example
     (a) If the contribution is primarily a new algorithm, the paper should make it clear how to reproduce that algorithm.
     (b) If the contribution is primarily a new model architecture, the paper should describe the architecture clearly and fully.
     (c) If the contribution is a new model (e.g., a large language model), then there should either be a way to access this model for reproducing the results or a way to reproduce the model (e.g., with an open-source dataset or instructions for how to construct the dataset).
     (d) We recognize that reproducibility may be tricky in some cases, in which case authors are welcome to describe the particular way they provide for reproducibility. In the case of closed-source models, it may be that access to the model is limited in some way (e.g., to registered users), but it should be possible for other researchers to have some path to reproducing or verifying the results.

5. **Open access to data and code**

   Question: Does the paper provide open access to the data and code, with sufficient instructions to faithfully reproduce the main experimental results, as described in supplemental material?

Answer: [Yes]

Justification: We will release the code needed to reproduce the results upon acceptance.

Guidelines:

- The answer NA means that paper does not include experiments requiring code.
- Please see the NeurIPS code and data submission guidelines (`https://nips.cc/public/guides/CodeSubmissionPolicy`) for more details.
- While we encourage the release of code and data, we understand that this might not be possible, so "No" is an acceptable answer. Papers cannot be rejected simply for not including code, unless this is central to the contribution (e.g., for a new open-source benchmark).
- The instructions should contain the exact command and environment needed to run to reproduce the results. See the NeurIPS code and data submission guidelines (`https://nips.cc/public/guides/CodeSubmissionPolicy`) for more details.
- The authors should provide instructions on data access and preparation, including how to access the raw data, preprocessed data, intermediate data, and generated data, etc.
- The authors should provide scripts to reproduce all experimental results for the new proposed method and baselines. If only a subset of experiments are reproducible, they should state which ones are omitted from the script and why.
- At submission time, to preserve anonymity, the authors should release anonymized versions (if applicable).
- Providing as much information as possible in supplemental material (appended to the paper) is recommended, but including URLs to data and code is permitted.

6. **Experimental setting/details**

   Question: Does the paper specify all the training and test details (e.g., data splits, hyper-parameters, how they were chosen, type of optimizer, etc.) necessary to understand the results?

   Answer: [Yes]

   Justification: The details of the experiments are provided Sec. 6.1,

   Guidelines:

   - The answer NA means that the paper does not include experiments.
   - The experimental setting should be presented in the core of the paper to a level of detail that is necessary to appreciate the results and make sense of them.
   - The full details can be provided either with the code, in appendix, or as supplemental material.

7. **Experiment statistical significance**

   Question: Does the paper report error bars suitably and correctly defined or other appropriate information about the statistical significance of the experiments?

   Answer: [Yes]

   Justification: We provide standard deviation for our method in Tab. 5 and Tab. 6. We also include std in the figures in Sec. 6.4.

   Guidelines:

   - The answer NA means that the paper does not include experiments.
   - The authors should answer "Yes" if the results are accompanied by error bars, confidence intervals, or statistical significance tests, at least for the experiments that support the main claims of the paper.
   - The factors of variability that the error bars are capturing should be clearly stated (for example, train/test split, initialization, random drawing of some parameter, or overall run with given experimental conditions).
   - The method for calculating the error bars should be explained (closed form formula, call to a library function, bootstrap, etc.)
   - The assumptions made should be given (e.g., Normally distributed errors).

- It should be clear whether the error bar is the standard deviation or the standard error of the mean.
- It is OK to report 1-sigma error bars, but one should state it. The authors should preferably report a 2-sigma error bar than state that they have a 96% CI, if the hypothesis of Normality of errors is not verified.
- For asymmetric distributions, the authors should be careful not to show in tables or figures symmetric error bars that would yield results that are out of range (e.g. negative error rates).
- If error bars are reported in tables or plots, The authors should explain in the text how they were calculated and reference the corresponding figures or tables in the text.

8. **Experiments compute resources**

   Question: For each experiment, does the paper provide sufficient information on the computer resources (type of compute workers, memory, time of execution) needed to reproduce the experiments?

   Answer: [Yes]

   Justification: As stated in Sec. 6.1, all experiments are conducted on a cluster with 3 A100 GPUs.

   Guidelines:

   - The answer NA means that the paper does not include experiments.
   - The paper should indicate the type of compute workers CPU or GPU, internal cluster, or cloud provider, including relevant memory and storage.
   - The paper should provide the amount of compute required for each of the individual experimental runs as well as estimate the total compute.
   - The paper should disclose whether the full research project required more compute than the experiments reported in the paper (e.g., preliminary or failed experiments that didn't make it into the paper).

9. **Code of ethics**

   Question: Does the research conducted in the paper conform, in every respect, with the NeurIPS Code of Ethics `https://neurips.cc/public/EthicsGuidelines`?

   Answer: [Yes]

   Justification: The research conducted in the paper conforms with the NeurIPS Code of Ethics.

   Guidelines:

   - The answer NA means that the authors have not reviewed the NeurIPS Code of Ethics.
   - If the authors answer No, they should explain the special circumstances that require a deviation from the Code of Ethics.
   - The authors should make sure to preserve anonymity (e.g., if there is a special consideration due to laws or regulations in their jurisdiction).

10. **Broader impacts**

    Question: Does the paper discuss both potential positive societal impacts and negative societal impacts of the work performed?

    Answer: [NA]

    Justification: This work focuses on point cloud assembly task. The author does not see any negative societal impact of this work.

    Guidelines:

    - The answer NA means that there is no societal impact of the work performed.
    - If the authors answer NA or No, they should explain why their work has no societal impact or why the paper does not address societal impact.
    - Examples of negative societal impacts include potential malicious or unintended uses (e.g., disinformation, generating fake profiles, surveillance), fairness considerations (e.g., deployment of technologies that could make decisions that unfairly impact specific groups), privacy considerations, and security considerations.

- The conference expects that many papers will be foundational research and not tied to particular applications, let alone deployments. However, if there is a direct path to any negative applications, the authors should point it out. For example, it is legitimate to point out that an improvement in the quality of generative models could be used to generate deepfakes for disinformation. On the other hand, it is not needed to point out that a generic algorithm for optimizing neural networks could enable people to train models that generate Deepfakes faster.
- The authors should consider possible harms that could arise when the technology is being used as intended and functioning correctly, harms that could arise when the technology is being used as intended but gives incorrect results, and harms following from (intentional or unintentional) misuse of the technology.
- If there are negative societal impacts, the authors could also discuss possible mitigation strategies (e.g., gated release of models, providing defenses in addition to attacks, mechanisms for monitoring misuse, mechanisms to monitor how a system learns from feedback over time, improving the efficiency and accessibility of ML).

11. **Safeguards**

    Question: Does the paper describe safeguards that have been put in place for responsible release of data or models that have a high risk for misuse (e.g., pretrained language models, image generators, or scraped datasets)?

    Answer: [NA]

    Justification: This work does not generate new data. The author does not see any risk of misuse.

    Guidelines:

    - The answer NA means that the paper poses no such risks.
    - Released models that have a high risk for misuse or dual-use should be released with necessary safeguards to allow for controlled use of the model, for example by requiring that users adhere to usage guidelines or restrictions to access the model or implementing safety filters.
    - Datasets that have been scraped from the Internet could pose safety risks. The authors should describe how they avoided releasing unsafe images.
    - We recognize that providing effective safeguards is challenging, and many papers do not require this, but we encourage authors to take this into account and make a best faith effort.

12. **Licenses for existing assets**

    Question: Are the creators or original owners of assets (e.g., code, data, models), used in the paper, properly credited and are the license and terms of use explicitly mentioned and properly respected?

    Answer: [Yes]

    Justification: This work used 3DMatch, BB and kitti datasets and cited them. The baseline methods are also cited.

    Guidelines:

    - The answer NA means that the paper does not use existing assets.
    - The authors should cite the original paper that produced the code package or dataset.
    - The authors should state which version of the asset is used and, if possible, include a URL.
    - The name of the license (e.g., CC-BY 4.0) should be included for each asset.
    - For scraped data from a particular source (e.g., website), the copyright and terms of service of that source should be provided.
    - If assets are released, the license, copyright information, and terms of use in the package should be provided. For popular datasets, `paperswithcode.com/datasets` has curated licenses for some datasets. Their licensing guide can help determine the license of a dataset.

- For existing datasets that are re-packaged, both the original license and the license of the derived asset (if it has changed) should be provided.
- If this information is not available online, the authors are encouraged to reach out to the asset's creators.

13. **New assets**

    Question: Are new assets introduced in the paper well documented and is the documentation provided alongside the assets?

    Answer: [NA]

    Justification: The paper does not release new assets.

    Guidelines:

    - The answer NA means that the paper does not release new assets.
    - Researchers should communicate the details of the dataset/code/model as part of their submissions via structured templates. This includes details about training, license, limitations, etc.
    - The paper should discuss whether and how consent was obtained from people whose asset is used.
    - At submission time, remember to anonymize your assets (if applicable). You can either create an anonymized URL or include an anonymized zip file.

14. **Crowdsourcing and research with human subjects**

    Question: For crowdsourcing experiments and research with human subjects, does the paper include the full text of instructions given to participants and screenshots, if applicable, as well as details about compensation (if any)?

    Answer: [NA]

    Justification: The paper does not involve crowdsourcing nor research with human subjects

    Guidelines:

    - The answer NA means that the paper does not involve crowdsourcing nor research with human subjects.
    - Including this information in the supplemental material is fine, but if the main contribution of the paper involves human subjects, then as much detail as possible should be included in the main paper.
    - According to the NeurIPS Code of Ethics, workers involved in data collection, curation, or other labor should be paid at least the minimum wage in the country of the data collector.

15. **Institutional review board (IRB) approvals or equivalent for research with human subjects**

    Question: Does the paper describe potential risks incurred by study participants, whether such risks were disclosed to the subjects, and whether Institutional Review Board (IRB) approvals (or an equivalent approval/review based on the requirements of your country or institution) were obtained?

    Answer: [NA]

    Justification: The paper does not involve crowdsourcing nor research with human subjects

    Guidelines:

    - The answer NA means that the paper does not involve crowdsourcing nor research with human subjects.
    - Depending on the country in which research is conducted, IRB approval (or equivalent) may be required for any human subjects research. If you obtained IRB approval, you should clearly state this in the paper.
    - We recognize that the procedures for this may vary significantly between institutions and locations, and we expect authors to adhere to the NeurIPS Code of Ethics and the guidelines for their institution.
    - For initial submissions, do not include any information that would break anonymity (if applicable), such as the institution conducting the review.

16. **Declaration of LLM usage**

Question: Does the paper describe the usage of LLMs if it is an important, original, or non-standard component of the core methods in this research? Note that if the LLM is used only for writing, editing, or formatting purposes and does not impact the core methodology, scientific rigorousness, or originality of the research, declaration is not required.

Answer: [NA]

Justification: The core method development in this research does not involve LLMs.

Guidelines:

- The answer NA means that the core method development in this research does not involve LLMs as any important, original, or non-standard components.
- Please refer to our LLM policy (`https://neurips.cc/Conferences/2025/LLM`) for what should or should not be described.